UNCLASSIFIED

SECURITY CLASSIFICATION OF THIS PAGE *(When Data Entered)*

REPORT DOCUMENTATION PAGE		READ INSTRUCTIONS BEFORE COMPLETING FORM
1. REPORT NUMBER NSWC TR 83-296	2. GOVT ACCESSION NO.	3. RECIPIENT'S CATALOG NUMBER
4. TITLE *(and Subtitle)* AN INEXPENSIVE VECTOR THIN FILM MAGNETOMETER		5. TYPE OF REPORT & PERIOD COVERED Final, Fiscal Year 1983
		6. PERFORMING ORG. REPORT NUMBER
7. AUTHOR(s) Paul E. Hunter, Leonard J. Schwee, Frank G. Salton, Mary T. Shephard		8. CONTRACT OR GRANT NUMBER(s)
9. PERFORMING ORGANIZATION NAME AND ADDRESS NAVAL SURFACE WEAPONS CENTER (Code R43) White Oak, Silver Spring, Maryland 20910		10. PROGRAM ELEMENT, PROJECT, TASK AREA & WORK UNIT NUMBERS 62766N F66112 ZF6611201 R02AA004
11. CONTROLLING OFFICE NAME AND ADDRESS		12. REPORT DATE 1 May 1984
		13. NUMBER OF PAGES 51
14. MONITORING AGENCY NAME & ADDRESS*(if different from Controlling Office)*		15. SECURITY CLASS. *(of this report)* UNCLASSIFIED
		15a. DECLASSIFICATION/DOWNGRADING SCHEDULE

16. DISTRIBUTION STATEMENT *(of this Report)*

Approved for public release; distribution unlimited.

17. DISTRIBUTION STATEMENT *(of the abstract entered in Block 20, if different from Report)*

18. SUPPLEMENTARY NOTES

19. KEY WORDS *(Continue on reverse side if necessary and identify by block number)*

Magnetometer; Thin Film Devices; Magnetic Field Detection; Magnetic Sensors; Permalloy Magnetometers; Magnetoresistance Magnetometers; Vector Magnetometers.

20. ABSTRACT *(Continue on reverse side if necessary and identify by block number)*

This report details the work performed in the 1983 fiscal year on a project oriented at producing thin film magnetometers. These sensors will prove to be very economical in mass production because of integrated circuit fabrication techniques used. The device is well characterized and its operation understood. Included in this report are data on its vector nature, linear dynamic range, biased field effects, thermal response and small field response. Finally, an application in ordnance round identification is described.

DD FORM 1 JAN 73 1473 EDITION OF 1 NOV 65 IS OBSOLETE

S/N 0102-LF-014-6601

UNCLASSIFIED

SECURITY CLASSIFICATION OF THIS PAGE *(When Data Entered)*

FOREWORD

This report describes the progress achieved in the 1983 fiscal year on a project directed at producing inexpensive thin film magnetic field sensors. This work was funded by the IED board of NSWC under task number 3R02AA004.

The device described in this document has been well characterized in most of its relevant operational parameters such as sensitivity and linearity. As such, it appears that at present it is suitable for applications such as the one described in Chapter Five. Also, there has been enough research done to point to the areas where improvements can most readily be made.

The authors wish to acknowledge the assistance provided by the following staff members of NSWC: Mr. Ray Goetz (R45), Mr. Martin Wirtz (R45), Mr. Richard Lundsten and Mr. John Scarzello (R43).

Approved by:

Ira M Blatstein

IRA M. BLATSTEIN, Head
Radiation Division

CONTENTS

ILLUSTRATIONS

ILLUSTRATIONS (Continued)

CHAPTER 1

INTRODUCTION

The detection of magnetic fields is a common function of many systems. Magnetometers of various types find their way into torpedoes, mines, buoys, intrusion detectors, vehicle detectors, and magnetic anomaly detectors to name a few systems. There are wide ranges in the field levels, dynamic ranges, and frequency of fields which must be detected. System level requirements impose constraints such as the maximum power consumption, the physical size and the environmental conditions. With such a broad "market" for magnetic field sensors, virtually any device which has performance advantages over others will find its technological niche.

The research described in this report concerns the concept, design, fabrication and characterization of a vector thin film magnetometer. The sensor element is physically very small and readily amenable to economical mass production techniques such as those used in the fabrication of integrated circuits. Indeed, it is easily conceivable that the necessary support electronics (amplifiers, for example) can be fabricated on the same substrate as the sensor, with an ensuing reduction in size and increase in reliability.

A previous thin film magnetometer covered in U. S. patent 3,405,355 by R. S. Hebbert provided the starting point for the device described in this report. The most important differences between the previous and current devices are the size reduction achieved with the thin film processing techniques employed and the higher impedance of the new device. The previous magnetometer was at least an order of magnitude larger in area and about 5% the impedance of the current design.

Chapter Two of this report explains a theoretical model for the performance of the magnetometer based on the Stoner-Wohlforth model of magnetization rotation. Chapter Three describes the design and fabrication process, and design tradeoffs are discussed. Chapter Four presents the characterization tests that have been performed. Chapter Five discusses a potential application of the magnetometer in ordnance round identification. Finally, Chapter Six covers several areas where improvements seem to be imminently possible.

CHAPTER 2

A THEORETICAL MODEL

In this chapter, we will present a simple model for the response of the thin film magnetometer to an applied field. The basis of the theory is the Stoner-Wolhforth coherent rotation model[1] which has been used to explain other devices such as the Crosstie random access memory and switching in thin films. However, this model does ignore such things as domain wall motion and edge effects. Consequently, one cannot derive a complete description of the magnetometer from this model. The model is, on the other hand, a convenient place to start.

UNIAXIAL ANISOTROPY

The magnetization (or average dipole moment per unit volume) in a thin film of permalloy lies in the plane of the film due to the large demagnetizing field which exists perpendicular to the film plane.[2] In the film plane, it is possible to create a preferred orientation for the magnetization during the deposition of the film.[3] In the absence of an external field, the magnetization will be along this axis, which is termed the easy axis. Consequently, the direction perpendicular to the easy axis is called the hard axis. Finally, as the magnetization can lie in either sense along the easy axis, the adjective uniaxial is attached (as opposed to unidirectional). Thus a film with a uniaxial anisotropy is one with an easy axis such that when there are no external fields present, the magnetization relaxes to the easy axis and the sense of the magnetization has no consequence on the energy of the magnetic state.

To rotate the magnetization away from the easy axis via an external field requires energy. In Figure 2-1, we depict the rotation of the magnetization away from the easy axis. In Figure 2-1a, the magnetization initially is along the easy axis but when a field is applied as in Figure 2-1b, the magnetization rotates to some angle, θ, such that there is an equilibrium between the torque which is trying to restore the magnetization to the easy axis and the torque exerted by the external field. The energy density associated with the uniaxial anisotropy is given by

$$E_A = K \sin^2 \theta \qquad (1)$$

where

K = anisotropy constant

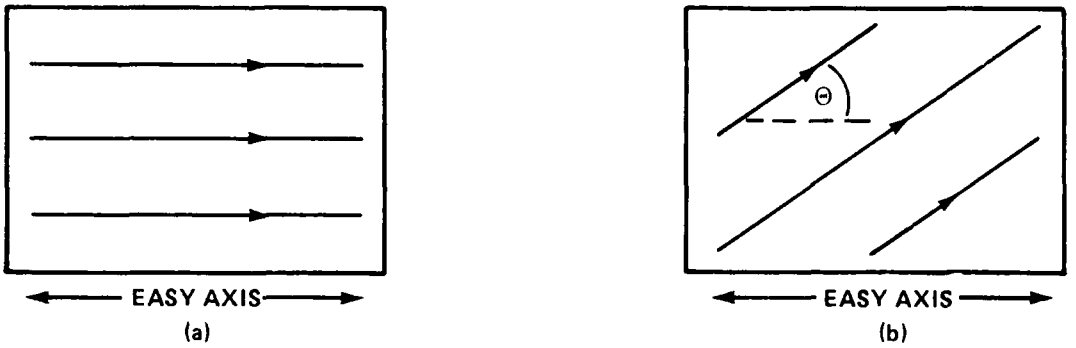

FIGURE 2-1. MAGNETIZATION IN A THIN FILM. (a) ZERO EXTERNAL FIELD. (b) EXTERNAL FIELD APPLIED.

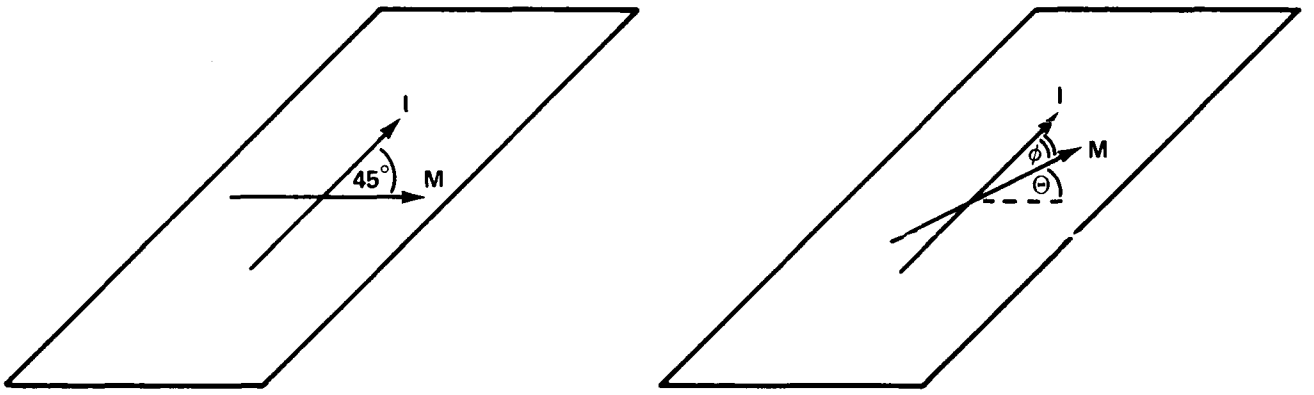

(a) $R = R_o + \frac{\Delta R}{2} \cos 2(45°)$

$= R_o$

(b) $R = R_o + \frac{\Delta R}{2} \cos 2(45° - \Theta)$

$= R_o + \frac{\Delta R}{2} \sin 2\Theta$

FIGURE 2-2. MAGNETORESISTANCE IN A THIN FILM ETCHED AT 45° TO THE EASY AXIS. (a) ZERO EXTERNAL FIELD. (b) EXTERNAL FIELD APPLIED.

and

θ = angle between the magnetization vector and the easy axis.

The energy density associated with the coupling of the magnetic moments to the applied field is

$$E_H = -\vec{M}\cdot\vec{H} \qquad (2)$$
$$= -H_x M\cos\theta - H_y M\sin\theta$$

where

M = magnetization

and

H_x, H_y = x and y components of the applied field.

The total energy in the model we have is given by the sum of the terms in equations (1) and (2). The equilibrium angle is obtained by minimizing this total energy with respect to the angle of rotation. In the general case we have presented so far, the resulting equation for the equilibrium angle is transcendental and requires a numerical solution. Consider however the case of simply a hard axis field ($H_x = 0$, $H_y = H$). Then the total energy is given by

$$E = K\sin^2\theta - MH\sin\theta \qquad (3)$$

and taking the derivative with respect to θ yields

$$0 = 2K\sin\theta\cos\theta - MH\cos\theta \qquad (4)$$
$$= (2K\sin\theta - MH)\cos\theta.$$

We define an equivalent field for the anisotropy as

$$H_K = 2K/M \qquad (5)$$

and thus find two solutions for the equilibrium angle:

$$\theta = \pi/2 \qquad (6)$$

or

$$\theta = \sin^{-1}(H/H_K). \qquad (7)$$

It is easy to verify that equation (7) gives the minimum energy result for $H < H_K$. For $H > H_K$, the solution is given by equation (6). This result gives an interpretation for H_K; the equivalent field denoted by H_K is the minimum magnetic field required to rotate the magnetization to the hard axis by a field which is solely along the hard axis. When a field of H_K or larger is applied along the hard direction, the magnetization saturates in this

direction.

Before leaving the topic of rotation, we note that for a small applied field, we can make the small angle approximation ($\sin x \approx x$) and obtain

$$\theta \approx H/H_K. \tag{8}$$

This approximation is better than 1% for $\theta \leq .24$ radians or 14^o.

MAGNETORESISTANCE

The rotation of the magnetization of a thin film must be detectable, preferably electronically, to produce a magnetometer. To observe this rotation, which is a linear response for small fields as demonstrated in equation (8), we utilize the anisotropic ferromagnetic magnetoresistance[4] that is found in thin films of permalloy and other materials. To explain this phenomena, we refer to Figure 2-2 which represents a thin film that has been etched such that a current flows at 45^o to the easy axis. The resistance to the current flow in the film is given by

$$R = R_o + \frac{\Delta R}{2} \cos 2\phi \tag{9}$$

where

R_o = resistance due to nonmagnetic effects,
ΔR = resistance attributable to the influence of the magnetization

and

ϕ = the smaller angle between the current vector and the magnetization vector.

Equation (9) shows that the resistance changes from a minimum value of $R_o - \Delta R/2$ at $\phi = 90^o$ through R_o at $\phi = 45^o$ and reaches a maximum of $R_o + \Delta R/2$ at $\phi = 0^o$.

MAGNETORESISTORS

The magnetoresistance effect allows us to now fabricate resistors which respond to magnetic fields. Figure 2-3 represents a thin film which has been etched to form two resistors which respond oppositely to an applied field. The resistors are utilized in a bridge circuit as shown, with a voltage V across the bridge and the output voltage e measured across the center taps. The legs opposite the magnetoresistors are some appropriately chosen standard resistors such that their value, R_o, is equal to the non-magnetic resistance of the magnetoresistors. To the power supply, the bridge looks like a simple resistance of R_o and draws a current of V/R_o.

The initial orientation of the magnetization is important if one wishes to have a vector magnetometer. If one wants the output simply proportional to the magnitude of the applied field, it only matters that it is initially oriented in the same direction in both legs.

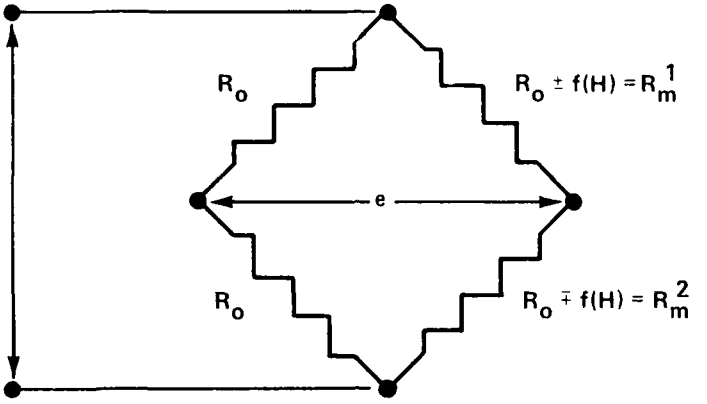

FIGURE 2-3. BRIDGE CIRCUIT WITH TWO MAGNETORESISTORS. THE RESISTANCE OF THE MAGNETORESISTORS VARIES WITH THE APPLIED FIELD, H.

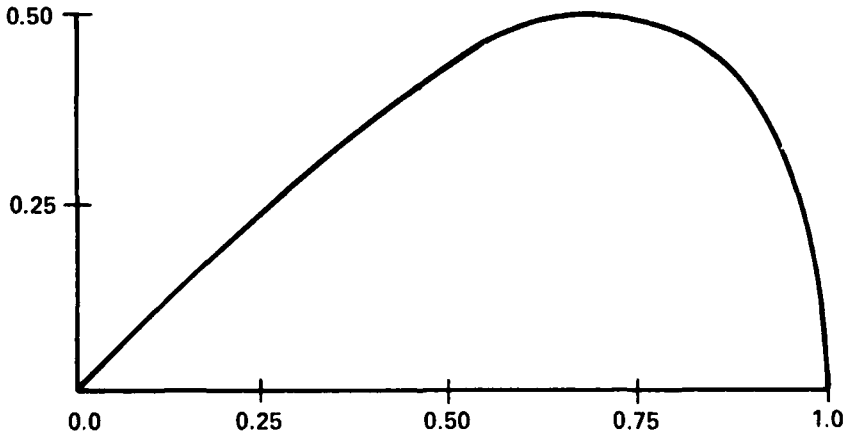

FIGURE 2-4. A PLOT OF THE FUNCTION $f(x)=x(1-x^2)^{1/2}$

In the absence of an applied field, the current and magnetization vectors are at 45^{o} to each other and consequently, the resistance of each magnetoresistor is R_o. Now, assume a small hard axis field is applied to the bridge. The magnetization thus rotates through some angle θ in both magnetoresistors of the bridge. Assume that the field is upwards in Figure 2-3. Then for R_m^1, the angle between the current and magnetization goes from 45^{o} to $45^{o} - \theta$. Thus we have

$$R_m^1 = R_o + \left(\frac{\Delta R}{2}\right)\cos\left[2(45^{o} - \theta)\right] \qquad (10)$$
$$= R_o + \frac{\Delta R}{2}\sin 2\theta.$$

Because we have chosen a field that is entirely along the hard axis, we can continue this derivation analytically. If the applied field were more general, with a component along the easy axis, we would be forced to start making small angle approximations at this point. Instead, we proceed with the exact solution and consider the more general case below. Thus, substituting equation (7) into equation (10) and using the identity

$$\sin 2A = 2 \sin A \,(1 - \sin^2 A)^{1/2}$$

we have

$$R_m^1 = R_o + \Delta R \left(\frac{H}{H_K}\right)\left(1 - (H/H_K)^2\right)^{1/2}. \qquad (11)$$

A plot of the function

$$f(x) = x(1-x^2)^{1/2}$$

is shown in Figure 2-4 for x in the range of 0 to 1. The maximum at x = .707 corresponds to the magnetization being rotated until it is parallel to the current. In this situation, the resistance is

$$R_m^1 = R_o + \frac{\Delta R}{2} \qquad (12)$$

which can be verified by substituting

$$H = H_K/\sqrt{2} \qquad (13)$$

into equation (11). The zero at $H = H_K$ (or x = 1) corresponds to saturation in the hard direction, in which case the current and magnetization are again at 45^{o}. Consequently, $R_m^1 = R_o$ in this case. Equation (11) also demonstrates the saturation effect. This equation only has a physical interpretation for $H \leq H_K$. For values of $H > H_K$, the solution becomes a complex quantity.

For small fields, we can linearize equation (11) and obtain

$$R_m^1 = R_o + \Delta R \left(\frac{H}{H_K}\right). \qquad (14)$$

This approximation will make an error of no more than 1% in the right hand term of equation (14) provided that

$$H/H_K < .12 \tag{15}$$

or that

$$\theta < 7^{\circ}. \tag{16}$$

The reason for the narrower restriction on θ in equation (16) than we had before (equation (8)) arises from the fact that the magnetoresistance responds as $\sin 2\theta$ rather than $\sin\theta$.

A similar derivation for R_m^2 of Figure 2-3 will produce

$$R_m^2 = R_o - \Delta R(\frac{H}{H_K}) \cdot \tag{17}$$

Thus as the resistance increases in one magnetoresistor of the bridge, it decreases in the other and the current through the magnetoresistors stays constant at $V/(2R_o)$.

We can now calculate the output signal, e, for the bridge. The current through both sides of the bridge stays constant at $V/(2R_o)$. Thus as R_m^1 changes with applied field H, we get

$$e = \frac{V}{2R_o}(R_o + \Delta R(\frac{H}{H_K})) - \frac{V}{2R_o}(R_o)$$

or

$$e = \frac{V}{2}(\frac{\Delta R}{R_o})(\frac{H}{H_K}) \cdot \tag{18}$$

This allows us to write for the sensitivity, S, of the basic magnetometer

$$S = \frac{e}{H} = \frac{V}{2}(\frac{\Delta R}{R_o})\frac{1}{H_K} \tag{19}$$

or, reducing it to a parameter that is normalized to the voltage that is impressed across the bridge, S′, we get

$$S' = \frac{S}{V} = \frac{1}{2}(\frac{\Delta R}{R_o})\frac{1}{H_K} \cdot \tag{20}$$

Recalling our definition of H_K, we have

$$S' = \frac{1}{2}(\frac{\Delta R}{R_o})\frac{M}{2K} \cdot \tag{21}$$

This last equation is very useful in understanding what produces the intrinsic sensitivity of the magnetometer. In the idealized theory we've presented (i.e., using the coherent rotation model) the sensitivity is related to three fundamental properties of the permalloy film: the magnetoresistance

ratio, $\Delta R/R_o$, the magnetization, M, and the anisotropy K. For the films we typically have used, $\Delta R/Ro$ is ~2% and H_K is ~3.5 Oe. Thus, the theoretical sensitivity would be

$$S' = \frac{1}{2}(.02)(\frac{1}{3.5Oe}) = .00286/Oe. \qquad (22)$$

For a voltage of 5V across the bridge, we predict

$$S = 5V \times S' = 14.3 \frac{mV}{Oe} .$$

In passing, we note that films with $(\Delta R/Ro) \sim 4\%$ have been reported[5] and the possibility remains of producing films with smaller anisotropy "fields" (ratios of K to M). Finally, one immediate improvement that can be made to improve the sensitivity is to use magnetoresistors in both legs of the bridge. In this case, we have

$$e = \frac{V}{2Ro}(R_o + \Delta R(\frac{H}{H_K})) - \frac{V}{2R_o}(R_o - \Delta R(\frac{H}{H_K})) \qquad (23)$$
$$= V(\frac{\Delta R}{Ro})\frac{H}{H_K},$$

or the output signal doubles for the same field without changing anything but the components of the bridge. This configuration is represented in Figure 2-5.

BIAS FIELDS

Several magnetometers based on the approach of the previous section have been fabricated and evaluated. However, during the development of the magnetometer, it became apparent that a permanent bias field along the hard axis could produce a more useful device. This new approach alleviated a few problems of the previous design and at the same time offered more flexibility. In this section, we will develop a theory (again based on the coherent rotation model) for the response of this new design. This derivation will then allow us to demonstrate what can be gained through using bias fields.

Consider a film where a hard axis bias field has been applied such that the thin film is saturated in the hard axis direction. The application of an external field at some orientation other than parallel to the hard axis will cause the magnetization to rotate away from the hard axis. For a field applied which is at an angle β to the easy axis, we can write

$$E_T = K\sin^2(\pi/2 - \delta) - \vec{M}\cdot\vec{H}_T \qquad (24)$$

where

E_T = total energy density,
δ = angle of rotation of $\vec{M}$ away from the hard axis
and
H_T = total field = sum of applied (H_A) and bias (H_B) fields.

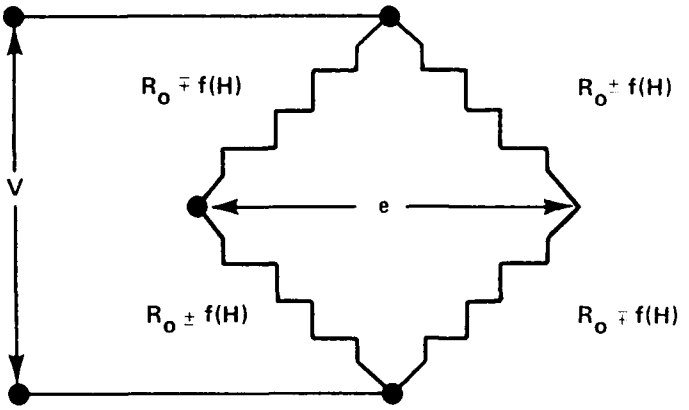

FIGURE 2-5. BRIDGE CIRCUIT WITH FOUR MAGNETORESISTORS. THIS CIRCUIT PRODUCES TWICE AS MUCH OUTPUT, E, FOR THE SAME APPLIED FIELD AS THE CIRCUIT OF FIGURE 2-3.

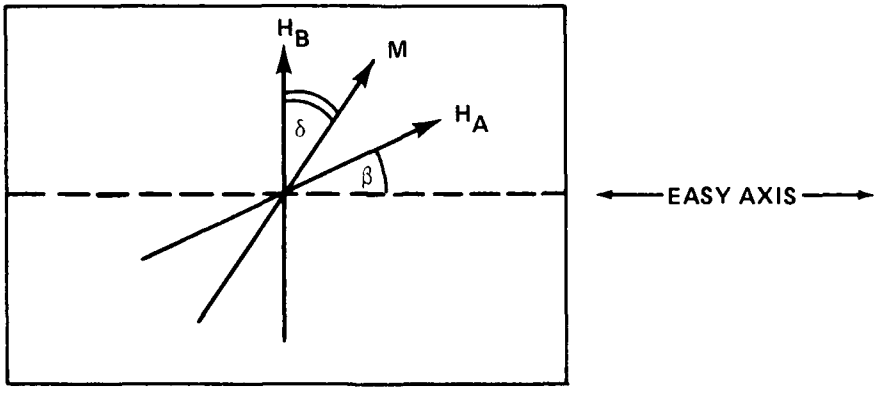

FIGURE 2-6. FILM WITH HARD AXIS BIAS FIELD. H_B = BIAS FIELD, H_A = APPLIED FIELD, M = MAGNETIZATION.

Referring to Figure 2-6, we can now write

$$E_T = K \sin^2(\pi/2 - \delta) - MH_B \cos\delta - MH_A \sin\beta\cos\delta - MH_A \cos\beta\sin\delta. \quad (25)$$

Minimizing this expression with respect to δ produces the equation for the new equilibrium angle. One obtains:

$$0 = -2K\cos\delta\sin\delta + MH_B\sin\delta + MH_A\sin\beta\sin\delta - MH_A\cos\beta\cos\delta. \quad (26)$$

Clearly this equation has no analytic solution for δ. Thus we approximate $\sin\delta \simeq \delta$ and $\cos\delta \simeq 1$ for small angles of rotation and, again using our definition of H_K, we have

$$\delta(H_K - H_B - H_A \sin\beta) \sim - H_A\cos\beta$$

or,

$$\delta \sim \frac{H_A \cos\beta}{H_B + H_A \sin\beta - H_K}. \quad (27)$$

We can readily write for the magnetoresistance

$$R = R_o + \frac{\Delta R}{2}\cos 2(45^o \mp \delta) = R_o \pm \Delta R \frac{H_A\cos\beta}{H_B + H_A\sin\beta - H_K} \quad (28)$$

and thus our output equation for a two magnetoresistor bridge is

$$e = \frac{V}{2}\left(\frac{\Delta R}{R_o}\right)\frac{H_A\cos\beta}{H_B + H_A\sin\beta - H_K}. \quad (29)$$

We note that if the applied field is along the easy axis (i.e., $\beta = 0$), equation (29) reduces to

$$e = \frac{V}{2}\left(\frac{\Delta R}{R_o}\right)\frac{H_A}{H_B - H_K}. \quad (30)$$

Before analyzing the results of this derivation, we note that equation (18) can be modified quite easily for a field that has a component along the easy axis as well as the hard axis to

$$e = \frac{V}{2}\left(\frac{\Delta R}{R_o}\right)\frac{H_A \sin\alpha}{H_K + H_A \cos\alpha} \qquad (31)$$

where α is the angle measured from the easy axis to the applied field direction. For $\alpha = \pi/2$, equation (31) reduces to equation (18).

Equations (29) and (31) most clearly illustrate the difference between the biased and unbiased magnetometers. We consider the bias field as an externally adjustable quantity whose value can be fixed during the fabrication of the magnetometer. Granted, H_B will be fixed once a device is produced, but one can still choose the optimum value for his application beforehand.

The anisotropy, however, is a consequence of the thin film fabrication process and the value can not vary very much, without producing undesirable changes in other film properties such as $\Delta R/R_o$. Thus in a biased film one has an extra control parameter that is lacking in an unbiased magnetometer.

The influence of the bias field is on the linear dynamic range, sensitivity, and vector response of the magnetometer.

Consider equation (31). We take H_K as fixed and consider the consequences. First, since we require a linear response, we must require

$$\frac{H_A \sin\alpha}{H_K + H_A \cos\alpha} < 0.12. \qquad (32)$$

(This equation is simply a more general form of equation (15).) For any angle α, (32) must hold but the worst case occurs when $\alpha = \pi/2$. Recalling that $H_K \simeq 3.5$Oe, we find that for the unbiased magnetometer, our linear response is limited to applied fields such that

$$H_A < (.12) \times (3.5\ \text{Oe}) \sim .40\text{e}. \qquad (33)$$

Thus we can expect a linear response in this situation to fields with a dynamic range of only $\pm$ .40e. However, we can expect the magnetometer to respond as a vector magnetometer for fields in its full dynamic range.

Letting H_A = .40e in equation (32) yields

$$\frac{\sin\alpha}{8.75 + \cos\alpha} \simeq \frac{\sin\alpha}{8.75}. \qquad (34)$$

Notice that if we allow larger possible values of H_A (or, a wider dynamic range), say $H_A = 1$, we can no longer ignore the $\cos\alpha$ term in the denominator of equation (32) and the vector response is lost.

Finally, we can see from equation (20) that the sensitivity varies inversely as H_K and there is no way to improve this relationship once H_K has been established by the deposition process.

Turning to equation (29), we can see the advantages of a bias field. Consider first the linearity requirement. From equation (27), we require

$$\delta = \frac{H_A \cos\beta}{H_B + H_A \sin\beta - H_K} < .12 \qquad (35)$$

which, for $\beta = 0$, becomes

$$\delta = \frac{H_A}{H_B - H_K} < .12. \qquad (36)$$

We see that we are no longer restricted by the anisotropy (H_K) of the film to produce a linear response over a given dynamic range. Instead, we can always choose some value of H_B that satisfies equation (36) to produce a response that is linear. For instance, let

$$H_B = 35 \text{ Oe} + H_K. \qquad (37)$$

Then equation (36) becomes

$$H_A < (.12)(35 \text{ Oe}) \simeq 4 \text{ Oe}$$

which is an order of magnitude better than our previous result.

The bias field can also be used to guarantee a vector response, that is, the output varies as $\cos\beta$, where β is the angle between the most sensitive direction (the easy axis direction for a film biased in the hard direction) and the direction of the applied field. To achieve this, one simply uses a bias field such that

$$H_B - H_K >> H_A . \qquad (38)$$

Finally, if one considers equation (29) for $\beta = 0$, it can be seen that choosing a bias of $H_B = H_K$ predicts a resonance in sensitivity. Of course higher order effects will prevent an infinitely sharp response, but there is the possiblity of producing a peaked response at this bias field. This should be a more sensitive operational mode than other possibilities (including zero bias field).

One final advantage associated with a bias field is control of the magnetization. A bias field large enough to saturate the magnetoresistors in the hard axis direction guarantees that stray fields will not upset a particular initial magnetization. In other words, whenever the device is "turned-on", it will be possible to know what the magnetization is. For an unbiased device, stray fields may leave the magnetization in some unpredictable state, such that the response to small fields to be measured may also be unpredictable.

THERMAL RESPONSE

Thus far in this discussion, it has been implicitly assumed that the change in resistance of a magnetoresistor is attributable only to a magnetic field. In reality, there are two quantities, R_o and ΔR, which are dependent on temperature. Equation (9) should be rewritten as

$$R = R_o(1+\alpha T)+ \frac{\Delta R(T)}{2} \cos 2\phi \qquad (39)$$

where

R = resistance of a magnetoresistor,
R_o = resistance at 0^oC,
α = thermal coefficient of resistance,
T = temperature,
ΔR = magnetoresistance coefficient,

and

ϕ = the angle between current and magnetization.

We assumed that the nonmagnetic term varies linearly with temperature. Measurement of α in the films used yields a value of

$$\alpha \sim 3{,}000 \text{ ppm}/^oC \qquad (40)$$

and the change in R_o is satisfactorily linear from 20^oC to 125^oC. The ΔR term, however, is more complicated in its thermal response. An exact model is not available, but we assume ΔR varies with the magnetization, M, and that M itself obeys the Bloch 3/2 power law. That is,

$$M(T) = M_o(1-(T'/Tc)^{3/2}), \qquad (41)$$

and

$$\Delta R \propto M \qquad (42)$$

so

$$\Delta R(T') = \Delta R(0)(1-(T'/Tc)^{3/2}), \qquad (43)$$

where

M_o = magnetization at 0^oK,
T' = temperature in degrees Kelvin,
Tc = Curie temperature

and

$\Delta R(0)$ = magnetoresistance coefficient at 0^oK.

To explore the ramifications of this model, we can write the response function for a saturating field ($H > H_K$) as

$$e = V \frac{\Delta R(T')}{R_o(T)} \tag{44}$$

and then determine how much signal is lost over some particular temperature range. We choose the military temperature specification of -50^oC to $+125^oC$. Thus we want to calculate

$$\frac{e(-50^o)-e(+125^o)}{e(-50^o)} \ . \tag{45}$$

The only parameter not given yet is Tc which we take as 560^oC. Then equation (45) predicts that 51.9% of the signal at -50^oC is lost at $+125^oC$.

A big improvement in this situation can be made if one makes use of a constant current source rather than a constant voltage source. Consider (44) rewritten as

$$e = \left(\frac{V}{R_o(T)}\right) \Delta R(T) = i(T)\Delta R(T) \tag{46}$$

where

$$i(T) = \frac{V}{R_o(T)} \ . \tag{47}$$

If one uses a current source such that i(T) is constant, then for the same temperature range as before, one has

$$\frac{e(-50^oC)-e(125^oC)}{e(-50^o)} = \frac{\Delta R(-50^oC)-\Delta R(125^oC)}{\Delta R(-50^oC)} \tag{48}$$

which predicts that 22.3% of the signal at -50^oC is lost at $+125^oC$.

The experiments performed to verify these predictions are reported in Chapter Four. The simple model used underestimates the $\Delta R(T)$ effect by about 10%. That is, a real device would loose about 24.7% of the signal due to temperature over the mil-spec range. However, the degradation is very linear and this facilitates compensating for the loss.

FIGURE OF MERIT

One can define a "figure of merit" for a magnetometer chip which is useful for comparing designs and focusing attention on those qualities which may most improve performance. What one usually wants is the most sensitive device for the least power. The power consumed (in a DC operational mode) of a magnetometer chip bridge is

$$P = i^2 R_o \tag{49}$$

while the sensitivity is given by equation (19). We define the figure of merit, m,

as

$$m = \frac{S}{P} = \frac{1}{i} \left(\frac{\Delta R}{R_o}\right) \frac{1}{H_B} , \tag{50}$$

where the factor of two has been dropped for simplicity. Since one would usually employ a bias field, H_K is replaced by H_B, which represents the bias field value. H_B should be as small as possible to maximize (50) yet still be large enough to satisfy the other criteria such as linear dynamic range. One then only has the magnetoresistance ratio of the magnetic film to work with, and this should be as large as possible. The figure of merit does improve as i^{-1} but the lower limit on i is fixed by the noise of the circuit. Also one will usually fix i well above the minimum value to maximize signal output. The upper limit, however, is set by the current density limit of the resistors (10^7 Amp/cm^2 for NiFe).

CHAPTER 3

DESIGN AND FABRICATION

In this chapter, we will discuss the design and fabrication of this thin film magnetometer. The design process requires the performance specifications of the assembled devices which are dictated by the particular application. The fabrication process is a typical thin film device procedure using photolithographic deposition and etching techniques.

DESIGN

To design a magnetometer, one requires at least the following characteristics: power consumption, linear dynamic range, acceptable chip size and sensitivity. Of course, one always desires the maximum sensitivity when starting out, but one frequently finds that a power versus sensitivity tradeoff must be made. As discussed in the previous chapter, the figure of merit for these devices is mostly a consequence of the magnetic film's properties, but the bias field can be adjusted to improve the sensitivity to power ratio.

To explain the design of a thin film magnetometer, we will consider a concrete example. We require the following characteristics: power consumption of less than 5 mW (also, we will use a 5 volt power supply), a sensitivity of at least 1 mV/Oersted (unamplifed), a dynamic range of ± 1 Oersted and a chip size of 150 mils on a side.

From the power specification we can calculate R_o. Using $P=V^2/R_o$, we find

$$R_o = (5V)^2/(5mW) = 5000 \text{ ohms.}$$

The sheet resistance of the 40nm permalloy used is 7.5 ohms per square, so we have

$$\begin{aligned} \#\text{ squares} &= 5000 \text{ ohms}/(7.5) \\ &= 667 \text{ squares.} \end{aligned}$$

Next, if we specify a design rule of 100 microns for the width, w, of the resistors, we find the required length, l, is given by

$$\begin{aligned} l &= \#\text{ squares} \times w \\ &= 66{,}700 \text{ microns} = 2626 \text{ mils.} \end{aligned}$$

Thus, the chip real estate required for each magnetoresistor is l x w or 10,339 mil^2. Assuming that we plan to put two resistors on each chip, the area we have available for one magnetoresistor is 11,250 mil^2. The ratio of required area to available area is 92%. This ratio is fairly high, but for this example, we'll assume that it is possible to layout the resistor pattern such that this density is achieved. A more conservative design would reconsider the constraints to achieve a ratio more like 75-80%.

Our requirement for a dynamic range of ± 1 Oersted forces a certain value for the bias field. From equation (36),

$$H_A/(H_B - H_k) < .12$$

and using

$$H_K = 3.5 \text{ Oe}, \quad H_A(\max) = 1.0 \text{ Gauss},$$

we find

$$H_B > (H_A/.12) + H_K = 11.8 \text{ Gauss}.$$

Using this value for the bias field, we can now check the sensitivity requirement. For the magnetoresistance ratio ($\Delta R/R_o$), we use .02. Then, from equation (30), our sensitivity is

$$S = \left(\frac{V}{2}\right) \frac{\Delta R}{R_o} \left(\frac{1}{H_B - H_K}\right)$$

$$= (2.5V)\ (.02)\ (8.3)^{-1}$$

$$= 6.0 \text{ mV/Oersted}.$$

Thus, using 5,000 ohm resistors and a bias field of 11.8 Gauss allows us to fabricate a magnetometer with the specified characteristics. If we had failed to meet the sensitivity requirements, one alternative would have been to consider using two chips as discussed in the previous chapter. But the requirements are met here with just one chip.

It must be mentioned at this point in the discussion that the full sensitivity predicted by equation (30) is never realized. There are demagnetizing effects which lower the effect of the applied field and this has not been accounted for in the simple rotation theory presented. Typically, the sensitivity is from 33% to 50% of the theoretical value. But if one multiplies the 6 mV/Oersted calculated above by .33, one still has enough sensitivity to meet the requirements of this exercise.

Now that we are satisfied that the specifications can be realized, the next step is to design the photomasks which will be used for the chip fabrication. Although we have a three layer device (permalloy, insulator and conductor), we need only two masks: one mask is used for etching the resistor pattern and the other is used both for creating vias in the insulator and etching bonding pads.

The mask is first laid out manually. This pattern is then reduced to a set of rectangles whose coordinates are referenced to a Cartesian plane. It requires a set of three cyclically ordered points to define a rectangle for the pattern generator (an Electromask 2000) which will expose the photomask. Before the mask can be produced each set of points must be converted to a new set of five numbers specifying the length, width, x-center, y-center and angular orientation of the rectangles. This data is then reformatted and stored on magnetic tape for later use on the pattern generator.

FABRICATION

Fabricating the chips for the thin film magnetometer consists of transfering the photomask image to a permalloy film, passivating the film and then depositing bonding pads of aluminum-copper. The substrates are then diced and good chips are mounted to leadless chip carriers. As this fabrication process does not require very fine linewidths or large chip areas, we expect a very high yield which translates to a low cost per chip. Our initial results are very encouraging and allow us to expect a yield of better than 90%.

The first and most critical processing stage is the deposition of the NiFe film. As a substrate, we use Corning glass sheets, which are 2" x 3" x 12 mil. The glass is cleaned with a commercial glass cleaning solution and then rinsed with deionized water. The resistivity of the water is 10 Mohm-cm or better.

Following a drying with N_2 gas, the substrate is mounted on a substrate holder and then placed in a vacuum chamber with a resistively heated deposition source. The chamber is evacuated to 10^{-6} Torr or lower and the glass is heated to 350°C before deposition begins. This temperature is maintained throughout the deposition.

During the initial melting of the material in the BeO crucible, the substrate is shielded from the source. The source material is NiFe bar stock. As we desire films of a zero magnetostriction composition, it is necessary to adjust the melt with pure Ni or Fe wire occassionally. The quantity of either element required is determined from a measurement of the change that stress produces in the anisotropy of the last film made.

Once the material has melted in the crucible, an initial deposition rate is measured using a Sloan quartz crystal rate monitor. From this measurement, we calculate the time needed to deposit a 40nm film. The substrate is pulled across an aperture to expose it to the beam of evaporated material. The required time of exposure dictates the speed that the substrate traverses the beam.

During deposition, a large DC magnetic field arising from Helmholtz coils mounted outside the chamber produces a well-defined easy axis in the film. Without this field, the easy axis would be unpredictable and possibly have a high degree of dispersion. Using the external field, a reproducible easy axis can be achieved.

After deposition, the film is allowed to cool in the chamber to reduce thermal stresses before it is removed. The film is then characterized to determine if all the necessary parameters have been produced. Using a nondestructive "Zappe" probe technique, the anisotropy , H_k, the coercivity, H_c, and the change in H_k due to stress are measured. Using a light transmission technique, the thickness of the thin permalloy film is also measured. If the film is acceptable, the next step is etching the permalloy.

Before we can transfer the mask image to the NiFe, the film must be cleaned and then coated with photoresist. The cleaning procedure begins with a deionized water bath in an ultrasonic agitator followed by a rinse with electronic grade propanol. Next, a mixture of 35% propanol and 65% freon in an ultrasonic bath degreases the film, with a final rinse in propanol. The precoating cleaning finishes with a baking at 100°C to evaporate any residual water. The film is ready to be coated with Shipley AZ1350J positive photoresist, which is used in all photolithography.

The resist is diluted 20% with the companion Shipley thinner and then is spin coated on the film. The resist is prebaked at 80°C for 30 minutes before exposure. Using a Cobilt CA-400 mask aligner, the film is brought in contact with the mask and then exposed for about 50 seconds. This long exposure is believed to be necessary because of the age of the optics in this machine.

After exposure, the resist is post-baked at 80°C for 30 minutes to harden the resist film and drive off any remaining volatiles. The permalloy film can now be etched. Using a mixture of diluted nitric and buffered hydrofluoric acids, the permalloy etches at a rate of 80 nm/min. The films have also been etched in an ion-milling machine (Commomwealth's Millatron) with satisfactory results. However, this is a more time-consuming process and, for our purposes, wet etching is preferable.

Following a resist stripping operation, the film is again cleaned as before. Another resist step follows where vias are to be defined in the passivating layer. Using the same Millatron, a target of Si_3N_4 is sputtered to deposit a layer of insulator. We have found that the layer deposited gives superior results if dry, research grade N_2 is leaked into the chamber during the process. The sample is then placed in a warm bath of acetone to "lift-off" the photoresist which defines the vias. This process is not always completely successful and it is believed that the heat that the photoresist experiences during the previous deposition is a significant factor here. Consequently, an effort is made to keep the sample as cool as possible during the silicon nitride deposition. Vacuum grease or some similar product has been found to aid the transfer of heat from the back side of the sample to the water-cooled deposition stage. We have also found that bypassing the post-exposure bake of the resist considerably improves the lift-off process yield. The resist does not have to be hardened for this process nearly as much as it does for etching.

If the lift-off operation has been reasonably successful, the deposition of AlCu (5% Cu) is carried out. The substrate is cleaned in a deionized water rinse to remove any particulates remaining after the lift-off. Using the ion beam coater once again, we deposit approximately 500nm of AlCu over the entire

substrate. This operation only requires that we rotate the target holder in the Millatron to place the metallization target in the ion beam for sputtering.

Once the AlCu has been deposited, we again coat the sample with photoresist and follow the expose and develop procedure as before. The same mask that was used for the via definition is used for this step. The reason that a new mask is not required is that in the via definition step, we did a lift-off. To produce bonding pads, we will use the photoresist for an etching mask.

After etching the sample in an etchant which only attacks the aluminum copper, we strip the remaining photoresist with acetone and inspect for defects. Assuming that no catastrophic failures are revealed at this point, the sample is then diced with a wafer scriber. Dies which survive this operation are then bonded to leadless ceramic chip carriers where one mil gold wire is used to make the electrical connection from the chip to the carrier.

ASSEMBLY

Testing the magnetometer chips requires that we incorporate them in a bridge circuit as described in the previous chapter. The resistance of the thin film magnetoresistors is easily measured once they are bonded to chip carriers. Having measured this value, R_o, standard nonmagnetic resistors are selected to match the magnetoresistors in the bridge. To reduce the noise in the circuit, it is desirable to use 1% thin film resistors for this purpose.

Since a small offset voltage arising from a resistance difference in the legs of the bridge can cause a severe problem in measuring the response of the magnetometer, it is useful to incorporate small, multi-turn trimpots in one or both legs of the bridge. The source of the imbalance may be from the contact resistances or poor matching of the magnetic and nonmagnetic resistors, but whatever the cause, if the bridge can not be zeroed in zero field, then attempting to amplify the output for small field detection will be difficult or impossible.

For intermediate and large level fields, it is only necessary to breadboard the chips and thin film resistors. However, electrical noise forces one to use a shield of some sort for low level signals. The standard 4" x 4" aluminum chassis works well for this purpose, allowing us to incorporate dry cells for power supplies. It is much easier to characterize the magnetometer's response using batteries, as rectified power supplies produce large amounts of noise on the signal at low levels.

Figure 3-1 shows a test circuit mounted in such a box. This chassis contains two batteries, one 4V and the other 12V, which are selectable with a toggle switch. Figure 3-2 shows a side view of the same test device. The signal is fed to the outside world through the insulated BNC Connector. The adjustment screws for multiturn trimpots which null the bridge for characterization are shown in the same figure. Figure 3-3a is a pictorial diagram of the circuit shown in Figure 3-1. Figure 3-3b is a schematic diagram of this circuit.

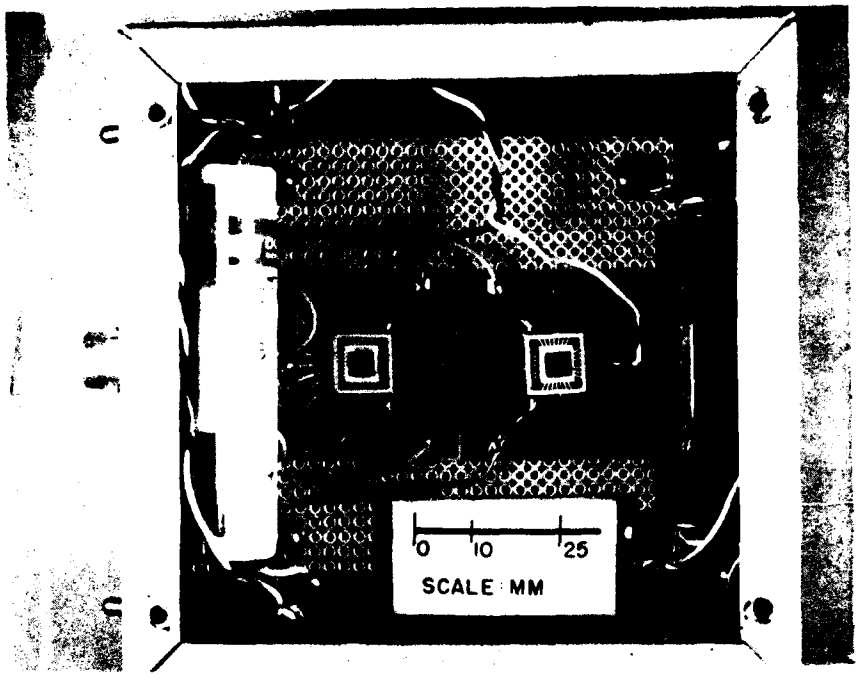

FIGURE 3-1. DOUBLE CHIP TEST CIRCUIT IN ALUMINUM CHASSIS, TOP VIEW

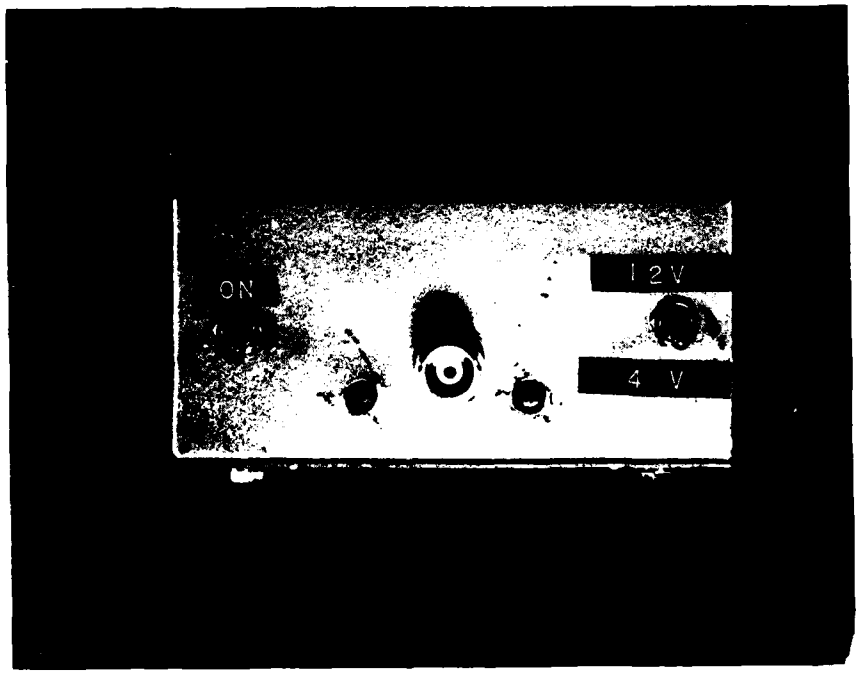

FIGURE 3-2. DOUBLE CHIP TEST CIRCUIT, SIDE VIEW

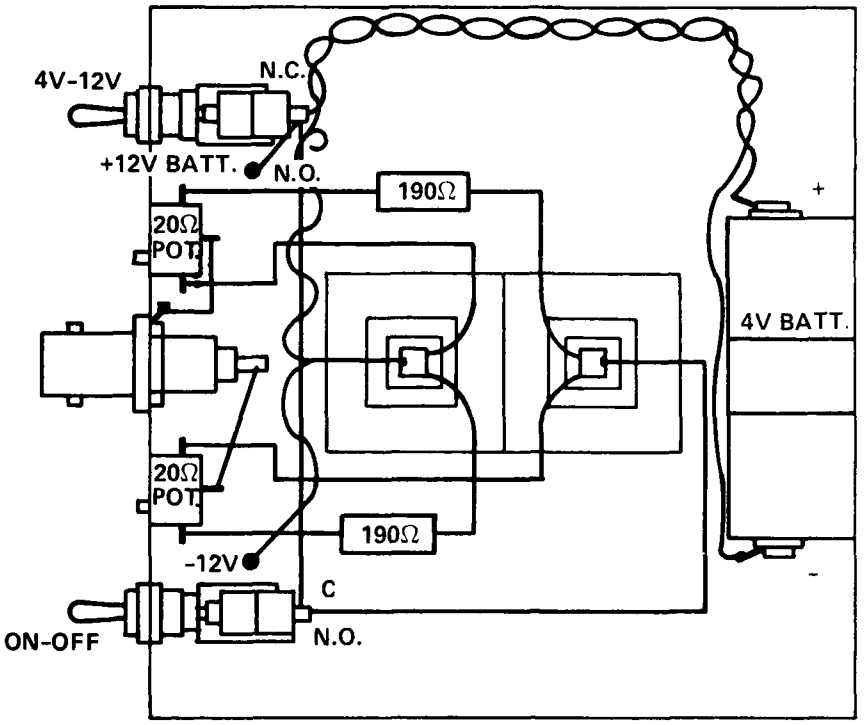

(a)

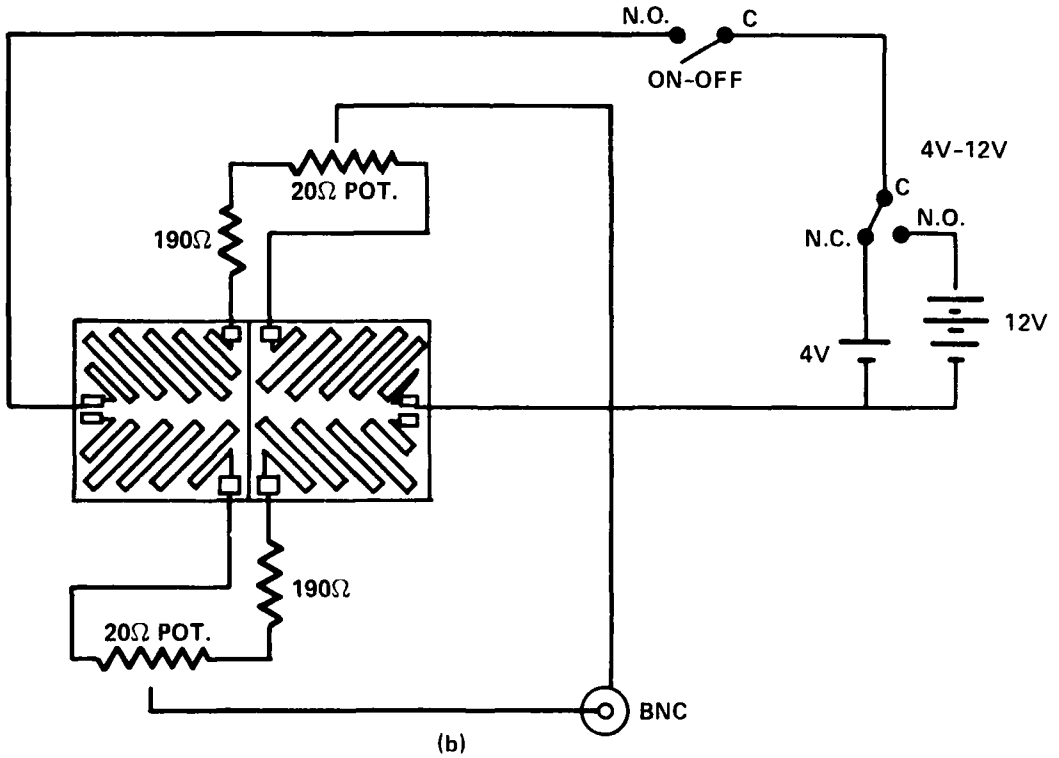

(b)

FIGURE 3-3. DOUBLE CHIP TEST CIRCUIT. (a) PICTORIAL DIAGRAM. (b) SCHEMATIC DIAGRAM.

CHAPTER 4

EXPERIMENTAL RESULTS

We will now describe the characterization tests which have been performed on the thin film magnetometer. These tests can be broken into five classes: biased sensitivity, linear dynamic range, vector response, thermal sensitivity and small field response (or signal to noise characteristics). Each will be discussed individually, but it should be recalled that a given result is not independent of all other parameters. For example, a larger bias field will produce a larger dynamic range but will also reduce the sensitivity.

Figure 4-1 is a response curve for a single chip magnetometer bridge. The voltage across the bridge is 5.0 volts supplied by a rectified power supply. The bias field was ~ 2Oe and the sensitivity was 2.6mV/Oe. The noise on the output was mostly due to the power supply and all results taken with batteries as power supplies were less noisy.

Whenever a value for sensitivity is given, it is important to keep in mind the applied voltage for this result. As was demonstrated in the theory section, the output will scale with the voltage across the bridge (or equivalently, the current through the bridge). This is clearly demonstrated in Figure 4-2 where the output voltage versus applied field is shown for two cases: the more sensitive bridge has 11.88 volts across it, while the less sensitive bridge has 4.04 volts across it. The ratios of sensitivities and applied voltages are both 2.94, verifying the scalability with voltage.

Equivalently, one could cite the sensitivity as 232 μV/V/Oersted (232 microvolts per volt per Oersted). But the value of the bias field must also be kept in mind. As the bias field does not have a linear influence on the sensitivity, one cannot normalize the response to a unit bias field.

BIAS FIELD CHARACTERIZATION

As the bias field greatly influences several other characteristics, we will discuss the result of these experiments first. The device tested was the circuit shown in Figure 3-1.

To simultaneously control the applied fields and bias fields, a set of perpendicular Helmholtz coils was used. The larger coil, used for the bias field, produced 37 Oersted per Ampere of current in the coil. The smaller coil, used for applied fields, yielded 3.2 Oersted per Ampere. The currents were controlled by observing the voltage drops across known resistors in series with the coils.

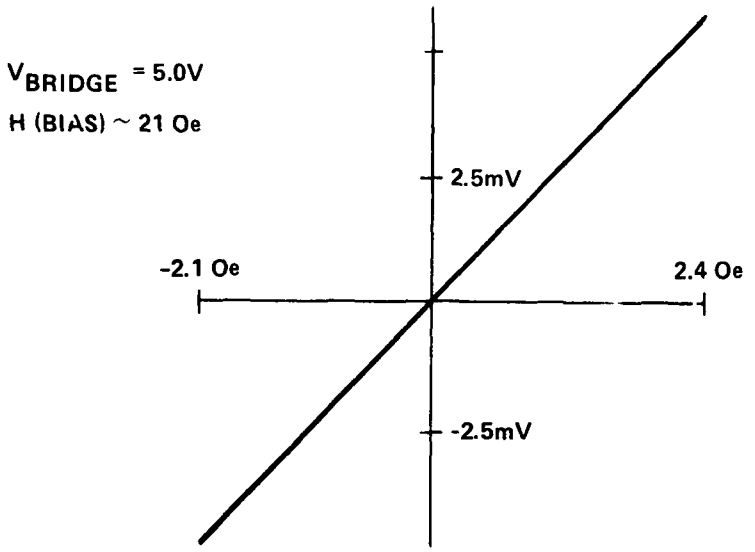

FIGURE 4-1. RESPONSE OF A SINGLE CHIP BRIDGE CIRCUIT

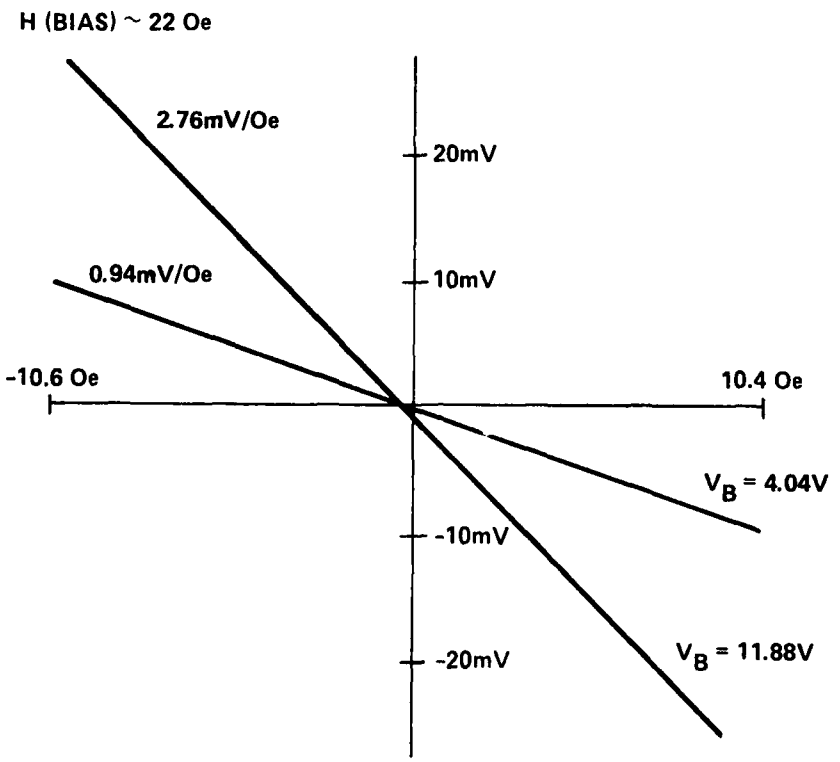

FIGURE 4-2. SENSITIVITY SCALING. (a) V(BRIDGE) = 11.88 VOLTS; SENSITIVITY = 2.76 mV/Oe. (b) V(BRIDGE) = 4.04 VOLTS; SENSITIVITY = 0.94 mV/Oe.

To produce an X-Y (field versus output voltage) curve as in Figure 4-1, the voltage across the applied field resistor was fed directly to the X-axis input of an HP model 7034A X-Y recorder, while the output from the bridge was fed to the Y-axis input. If the signal was too small to directly drive the Y-axis, the signal was amplified with a Princeton Applied Research model 113 amplifier.

Figure 4-3 is a typical plot of the result for a sensitivity versus bias field experiment, with the bias field along the hard axis. Figure 4-4 is a similar curve showing the effect of an easy axis bias field with hard axis applied fields. As could be anticipated, the two curves are very similar for large values of bias field. According to the theory developed in Chapter Two, the sensitivity for a hard axis bias varies as

$$S \propto (H_B - H_K)^{-1} \tag{51}$$

while for an easy axis bias, it varies as

$$S \propto (H_B + H_K)^{-1} \tag{52}$$

When the bias field is much greater than the equivalent anisotropy field, both results become

$$S \propto H_B^{-1} \tag{53}$$

We note that the sensitivity for a hard axis bias field is slightly greater for larger fields than the sensitivity for an easy axis bias field, as one would expect from equations (51) and (52).

For small values of the bias field, the situation is much more difficult to analyze and the results for small fields should not be taken too faithfully. The main problem with the small field regime is the spurious external fields which invalidate results in this region. Sources of such fields are the earth's field and the presence of permeable material in the environment.

Both the measurements given in Figures 4-3 and 4-4 were also done with bias field 180° opposed to the fields used to produce these graphs. The results were identical except for a change in the sign of the output voltage. The magnitudes of the outputs stayed the same.

LINEAR DYNAMIC RANGE

The curves presented in Figure 4-5 demonstrate the influence of the bias field on the linear dynamic range. For this experiment, we wished to produce an output that was linear from 0 to + 6 Oersteds. Using the crossed-coils as

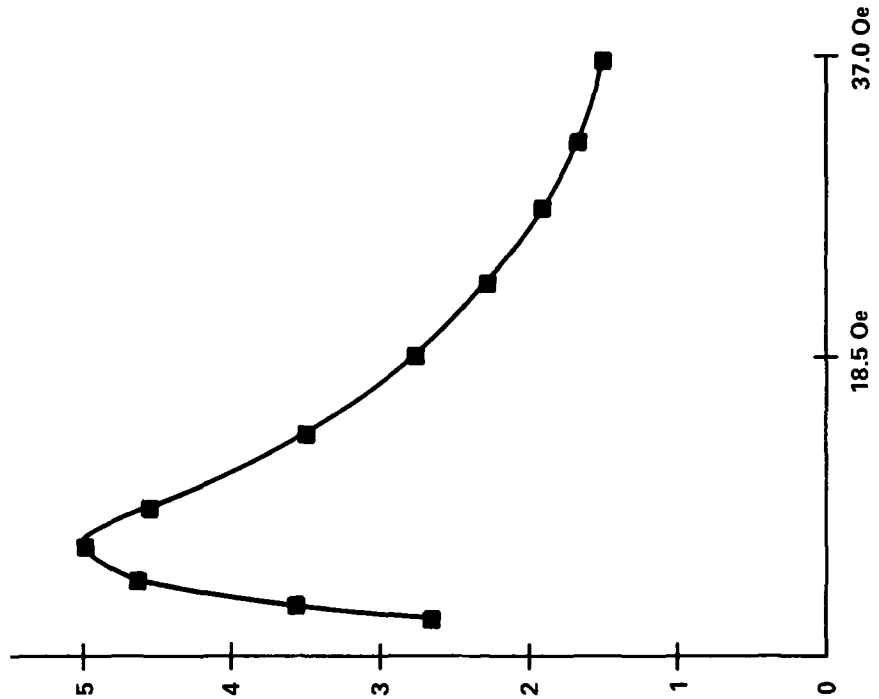

FIGURE 4-3. SENSITIVITY (mV/Oe) VS. HARD AXIS BIAS FIELD, V(BRIDGE) = 4 VOLTS

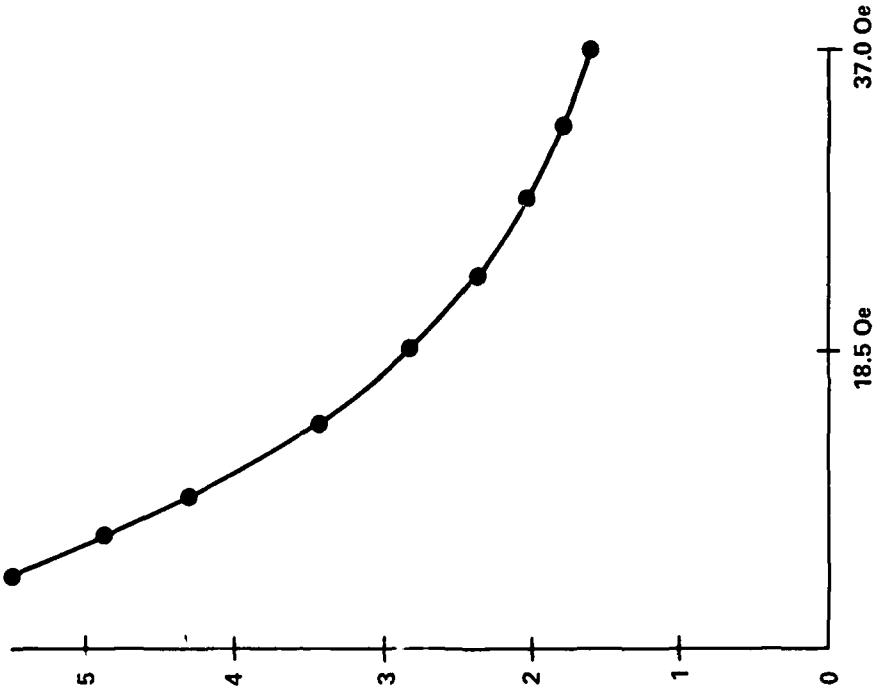

FIGURE 4-4. SENSITIVITY (mV/Oe) VS. EASY AXIS BIAS FIELD, V(BRIDGE) = 4 VOLTS

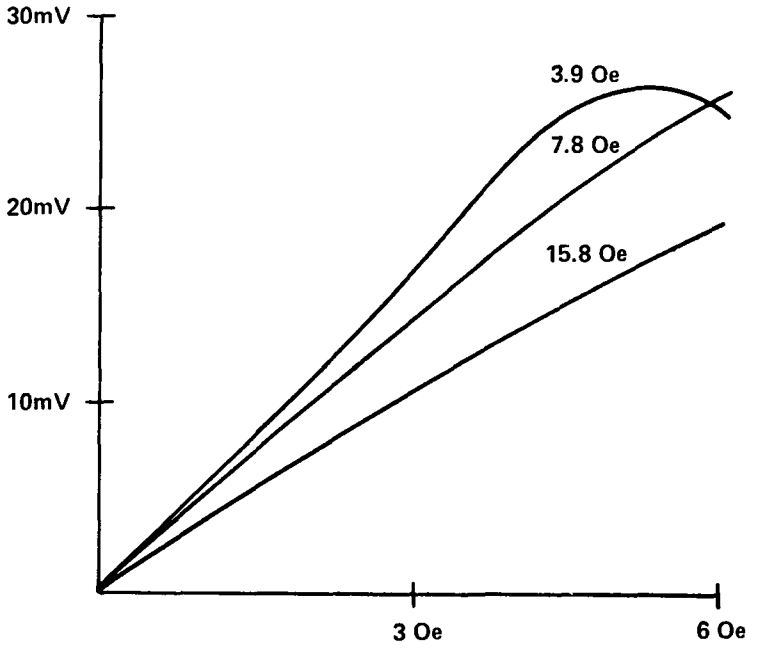

FIGURE 4-5. INFLUENCE OF BIAS FIELD ON LINEARITY. DOUBLE CHIP BRIDGE; V(BRIDGE) = 4 VOLTS.

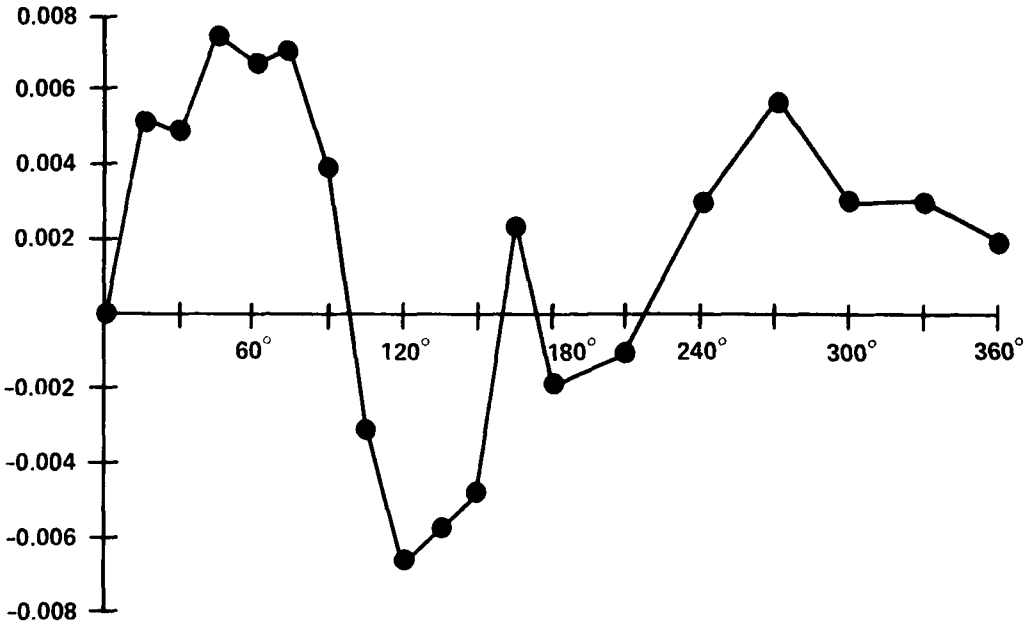

FIGURE 4-6. VECTOR RESPONSE OF A DOUBLE CHIP BRIDGE. THIS CURVE IS A PLOT OF $s(\theta)/s(0^\circ)$-COS(θ). THE LARGEST DEVIATION FROM THE COSINE FUNCTION IS 0.0077.

before, the applied field range was fixed and the biased field was set at three different values. The first curve, with a bias of 3.9 Oe, is very reminiscent of Figure 2-4. Clearly, we hadn't achieved full linearity with this bias, so more bias was applied.

In the next two curves, the suppression of the sensitivity we discussed in the previous section is evident, but the increasing linearity also occurs. The final run (with 15.8 Oe bias) is sufficiently linear for demonstration, but this bias field is not large enough to meet the criterion of equation (36). Thus, it is noticeable that this curve deviates slightly near the upper limit of applied field from a linear response. One would need a bias field of about 60 Oe to satisfy a 1% deviation limit.

VECTOR RESPONSE

As was explained in the theory chapter, this thin film magnetometer should behave as a vector magnetometer. That is, the output should be proportional to cos θ where θ is the angle between the applied field and the sensitive axis of the magnetometer. Equivalently, as the angle between the applied field and sensitive axis increases, the output will only correspond to the component of the applied field along the sensitive axis.

To demonstrate this, a different experimental set up was required. A much larger set of Helmholtz coils was obtained which produced 1.12 Oersted per Ampere. To bias the magnetometer, two permanent magnets were fixed to a lucite slab to which the chassis containing the circuit under test was also attached. The magnets produced a field of about 20 Oersted at the magnetoresistors. Referencing the lucite to a piece of polar graph paper permanently fixed with respect to the coils allowed us to establish the angle between the applied field and the sensitive direction of the circuit. That is, the magnetometer was moved in the field fixed in space and its sensitivity as a function of angle was determined. Equivalently, one could fix the magnetometer in space and move the coils (and thus reorient the field).

The experimental results of the vector response measurements are presented in Figure 4-6. As the ratio

$$S(\theta)/S(0^{o}) \qquad (54)$$

corresponded very closely to $\cos(\theta)$, as expected, the most meaningful way to present the results was to plot the difference between the ratio represented by (54) and $\cos(\theta)$. The largest difference is .0077 and the difference appears to be mostly due to noise in the measured signal and experimental error. The fact that there is still some sensitivity when the magnetometer is theoretically perpendicular to the applied field (i.e., at 90^{o} or 270^{o}) is indicative of small ambient fields which are not shielded out and which become significant when the applied field is small.

Clearly, the response varies with the component of the applied field along the sensitive axis. But it should be emphasized again that this is the case only when the bias field is significantly greater than the component of the

applied field along the bias direction; that is, so long as equation (38) is valid.

THERMAL RESPONSE

In order to determine the thermal response of this thin film magnetometer, several tests have been performed over the temperature range of $+20^{o}C$ to $+120^{o}C$. The devices were placed in a Blue M oven normally used for baking purposes during processing. The temperature was measured with an HP quartz thermometer (Model 2801A) and measurements were taken every $10^{o}C$.

First, to determine the linear coefficient of resistance of a magnetoresistor, note that for a resistor that has been saturated such that the current is parallel to the magnetization, one gets

$$R(T) = R_o(T) + \frac{\Delta R(T)}{2} \tag{55}$$

while if the resistor is saturated with the current and magnetization being perpendicular, one gets

$$R(T) = R_o(T) - \frac{\Delta R(T)}{2} \tag{56}$$

Thus, one can obtain $R_o(T)$ and $\Delta R(T)$ by taking the average and difference of equations (55) and (56) respectively. The data taken during two of these experiments are presented in Figures 4-7 and 4-8. Using a linear regression curve fitting routine supplied with the Standard Pac for an HP 67 calculator, one finds that $R_o(T)$ takes the form

$$R_o(T) = R_o(0^{o}C)\ (1 + \alpha T) \tag{57}$$

where

α = linear coefficient of resistance

= 3,031 ppm/^{o}C

and $\Delta R(T)$ takes the form

$$\Delta R(T) = \Delta R(0^{o}C)\ (1-\beta T) \tag{58}$$

where

β = 1,342 ppm/^{o}C

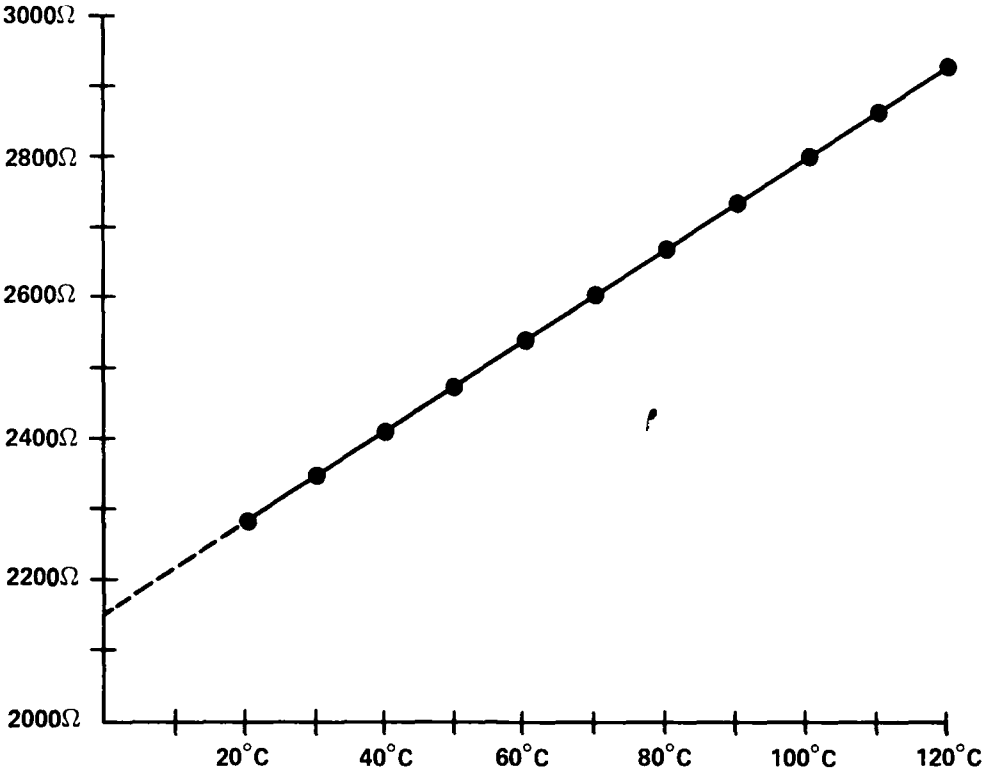

FIGURE 4-7. TEMPERATURE DEPENDENCE OF R_o (T)

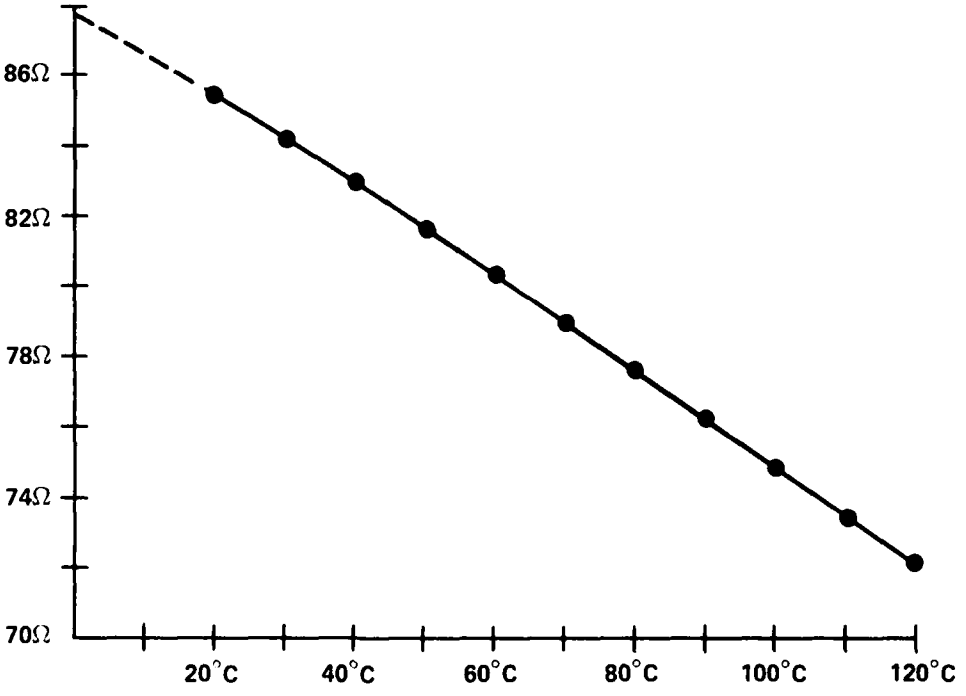

FIGURE 4-8. TEMPERATURE DEPENDENCE OF ΔR(T)

to a high degree of correlation on this temperature range. The correlation coefficients are .9996 and .9989 for $R_o(T)$ and $\Delta R(T)$, respectively. (A perfectly linear relationship would have a correlation coefficient of exactly one.)

Equation (58) for ΔR of T does not have exactly the same form as was assumed in the theory section, but if one considers the small range of 100^oC for which the data was taken, then a linear fit to equation (43) is reasonable. If one assumes a relationship for ΔR such as

$$\Delta R(T) = \Delta R(0^oC)\ (1-(T/T_c)) \tag{59}$$

where T_c is the Curie temperature as before, then the association that

$$\beta \simeq T_c^{-1}$$

can be made. If one takes 560^oC for T_c, then

$$T_c^{-1} = 1{,}786\ ppm/^oC.$$

It is not surprising that T_c^{-1} is significantly different from β above. The actual magnetization is vanishing faster than linearly with temperature. Thus a linear fit to the data predicts an erroneously large Curie temperature, which is equivalent to β being smaller than T_c^{-1}.

A more interesting result was obtained when we attempted to verify that a constant current source would alleviate the signal loss from the increase in $R_o(T)$. A bridge was made by dicing a sample such that two chips remained on the same substrate. Then the chips were bonded to form a bridge that was composed only of magnetoresistors. This configuration is shown in Figure 4-9.

The same chip was used to measure the saturation output for two different experiments. In the first, a constant voltage was maintained across the chip of $5.000 \pm .0001$ volts. In this case, the saturation output as a function of temperature is given by

$$e = \pm V\ (\frac{\Delta R\ (T)}{R_o(T)}). \tag{60}$$

In the second experiment, a constant current of $1.000 \pm .003$ mA was supplied to the bridge. The output in this case is

$$e = \pm I\ (\Delta R\ (T)). \tag{61}$$

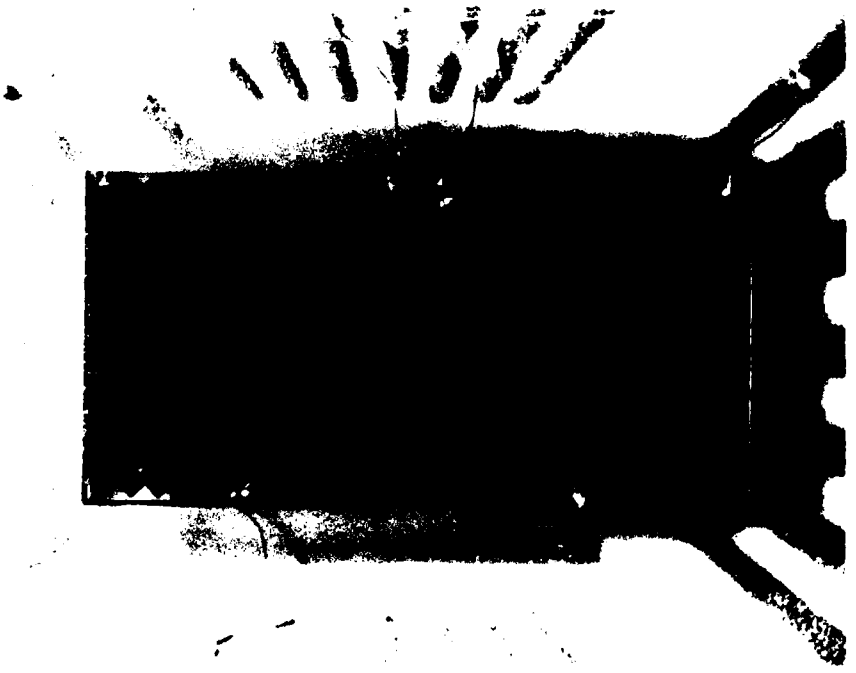

FIGURE 4-9. DOUBLE CHIP BRIDGE ON A SINGLE SUBSTRATE

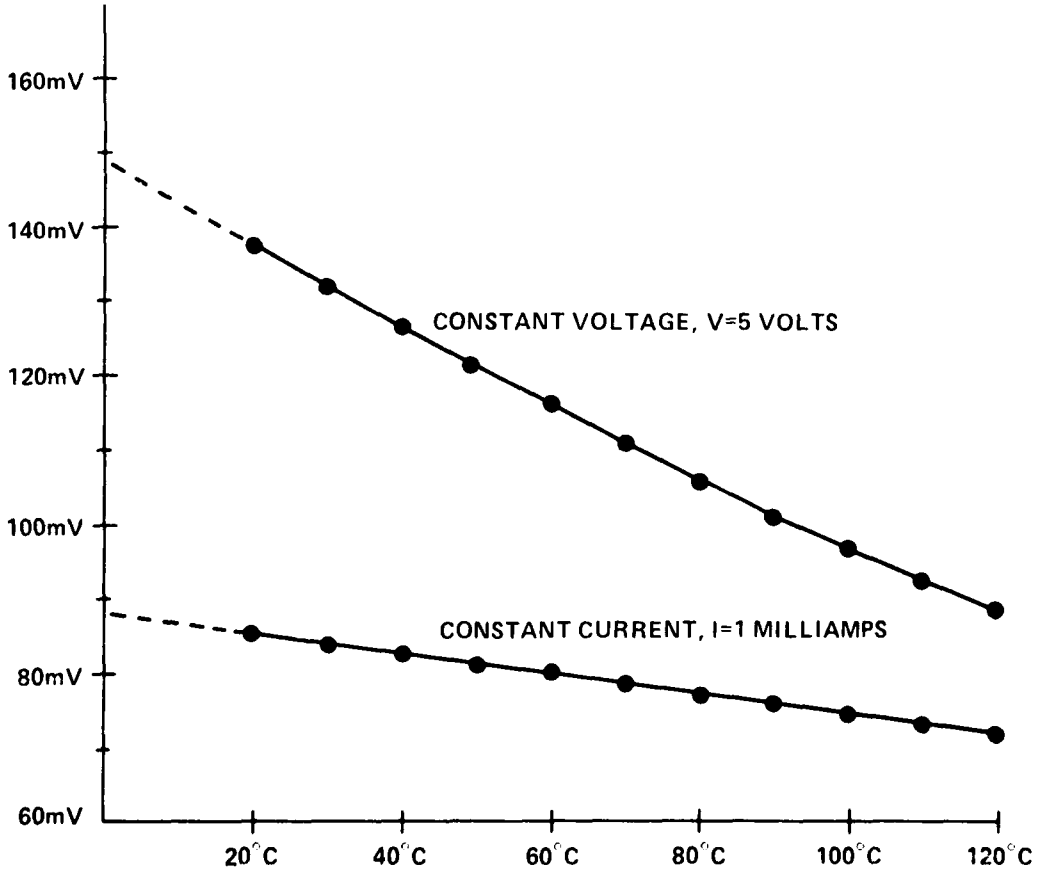

FIGURE 4-10. COMPARISON OF CONSTANT VOLTAGE SOURCE BRIDGE TO CONSTANT CURRENT SOURCE BRIDGE

The results are shown in Figure 4-10. Again, the temperature range is $+20^{o}C$ to $+120^{o}C$, with the behavior for temperatures less than $20^{o}C$ indicated by a linear extrapolation of the higher temperature measurements.

For the constant voltage case, if one computes

$$\frac{e(20^{o}C) - e(120^{o}C)}{e(20^{o}C)} \qquad (62)$$

for the data presented in Figure 4-10, then one finds that 36.5% of the signal at $20^{o}C$ is lost at $120^{o}C$. However, if one uses equation (62) for the constant current case, then one finds that 15.7% of the signal is lost. If one calculates the signal loss for these two cases using the theory of Chapter Two for these cases, then when the voltage is kept constant, 33.4% of the signal is predicted to be lost while for the constant current case, the prediction is 14.6%.

There is no crossing of the curves in Figure 4-10 by design, but if one wishes to compare the behavior of the two techniques starting from the same initial operating point, say $20^{o}C$, then one need only rescale either curve as we demonstrated in Figure 4-2.

SMALL FIELDS AND NOISE

In order to determine the behavior of our thin film magnetometer in small fields and to establish a DC noise level, a double chip bridge like the one shown in Figure 4-9 was placed in a shielded container which housed a calibrated coil arrangement. The bridge was biased with approximately 20 Oe and subjected to a 48 gamma peak to peak field at 0.1 Hz. The voltage across the bridge was 5.4 V from a battery power supply and the bridge drew approximately 1.8 mA of current.

The results are shown in Figure 4-11. The bridge did clearly respond to the input signal. To produce the output signal, it required an amplification of 10,000X. But, this is as expected from the sensitivity at 5.4V and 20 Oe bias.

Finally, the DC noise is producing spurious signals of at most 15 gamma. Thus, we take 15 gamma as the worst case DC noise.

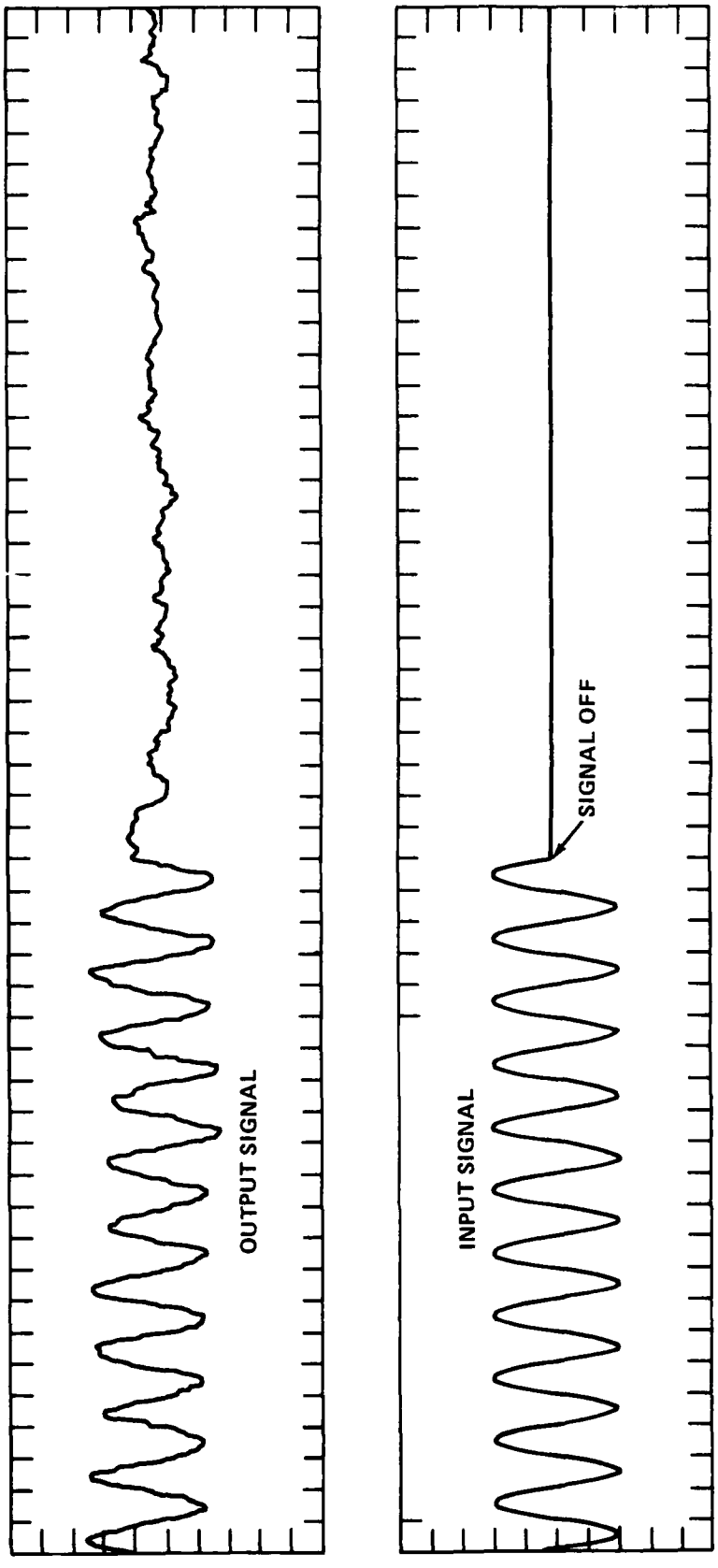

FIGURE 4-11. SMALL FIELD LEVEL OUTPUT. INPUT SIGNAL = 48 GAMMA (PEAK TO PEAK). OUTPUT SIGNAL ~1.8 μV (PEAK TO PEAK). SENSITIVITY ~3.75 mV/Oe OR 37.5 nV/GAMMA. NOISE DUE TO MAGNETOMETER CIRCUIT ~15 GAMMA. INPUT SIGNAL FREQUENCY = 0.1 Hz. BIAS FIELD ~20 Oe. V(BRIDGE) = 5.4 V.

CHAPTER 5

ORDNANCE ROUND IDENTIFICATION: AN APPLICATION

During the development of the vector thin film magnetometer, one application that arose is ordnance round identification via magnetic coding. The basic concept involves attaching permanent magnets to ordnance rounds in such a way that the field produced is detectable when the round is situated in its firing mechanism. The detection of such fields facilitates round identification as well as determining a simple loaded or unloaded condition. Performing this function electronically enables one to transmit this information reliably to a fire control computer.

The implementation of this concept has been discussed in detail in reference 6. The application discussed is the six tube MK 137 launcher (Super RBOC), which is used to protect surface combatants by launching any of a variety of decoy rounds. Having more than one possible round to fire from a given launcher, the fire control computer must have accurate knowledge of the location of all possible rounds. Thus it is mandatory that a round identify itself to the computer once it is deployed, and the most accurate way to do this is electronically. The uncertainty and extra time delay associated with "a man in the loop" implementation is unacceptable in any realistic scenario.

Unfortunately, no direct contact can be made to the round in the launcher tube. The environment such a connector must survive, particularly when the round is fired, is too severe for reliable electrical connection. Equally important is the prospect that an electrical connector may interfere with the launching of the round. Thus one must back off from any direct contact mechanism and look for other approaches.

Of the possible signatures a round might have in a launcher tube, a magnetic field appears to be an ideal one to use for identification. The field can easily be generated from sources (permanent magnets) which (1) consume no power, (2) aren't affected by ambient conditions and (3) don't interfere with any other functions of the round. There are ambient fields to be accounted for, but one can utilize magnets which produce fields sufficiently large to reduce ambient fields to noise.

The sensor discussed in reference 6 is a Brown ring core magnetometer. This device, while functionally suitable for the identification scheme proposed, was considered too expensive. The vector thin film magnetometer described in this report is much less expensive for the basic sensor, and would occupy less space than the previous sensor.

With these thoughts in mind, we set out to test a vector thin film magnetometer for this application. Guided by Figure 8 of reference 6, which is reproduced in this document in Figure 5-1, we tested the circuit of Figure 3-1 in a field of ±20 Oersteds. Equation (36) dictated that a bias field of approximately

$$H_B > (H_A/.12) + H_K$$

$$\approx 20\ \text{Oe}/.12 = 167\ \text{Oe}$$

was required.

With this much bias, we elected to use the 12V battery in the circuit. In this particular application, minimizing power was much less important than maximizing sensitivity. The results are shown in Figure 5-2. It must be emphasized that the output from the sensor is not amplified. The sensitivity is approximately 0.87 mV/Oersted. To bring the sensitivity up to the level indicated by Figure 5-1 requires an amplification of about 172, certainly a value within reach of common single stage operational amplifier circuits.

Thus, we conclude that the vector thin film magnetometer is suitable for this application. Using a constant current source, one compensates for most of the thermal degradation of the signal. The remaining thermal effect exhibited by ΔR would cause an uncertainty of 20% over the full mil spec range, or ±10% for a normal operating point. Field levels in this application can reduce this uncertainty to an inconsequential amount. That is, as one would be looking for discrete levels, say ±5 Oe and ±10 Oe, a fluctuation of 10% in either direction will not prevent distinguishing these field levels.

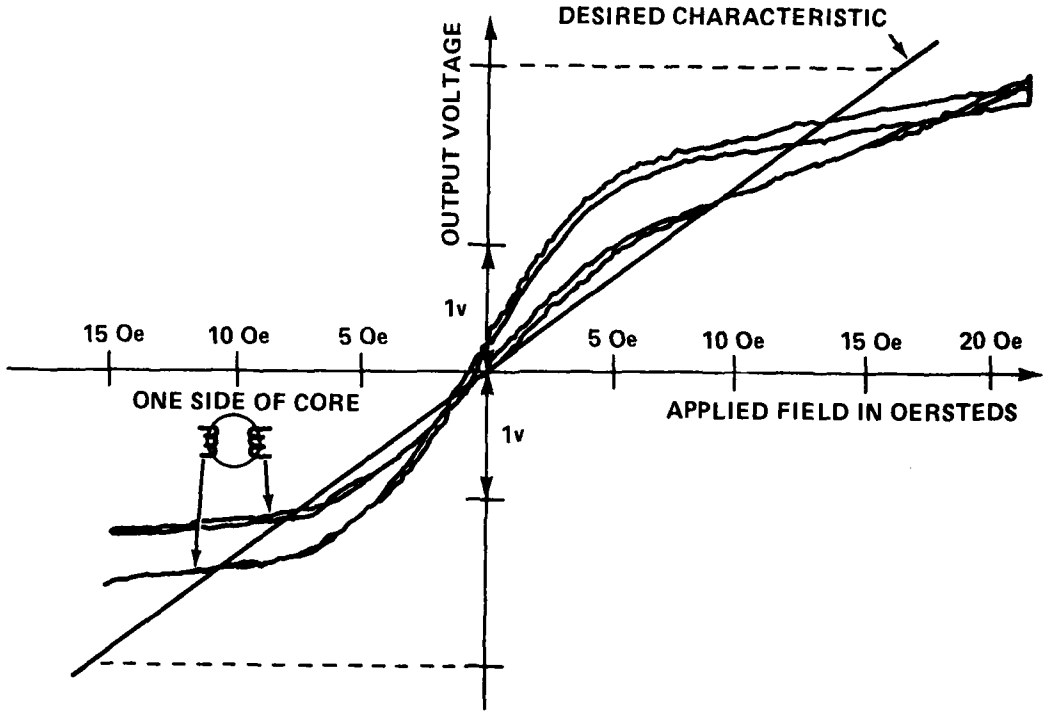

FIGURE 5-1. DYNAMIC RANGE OF PROTOTYPE SENSOR # 1

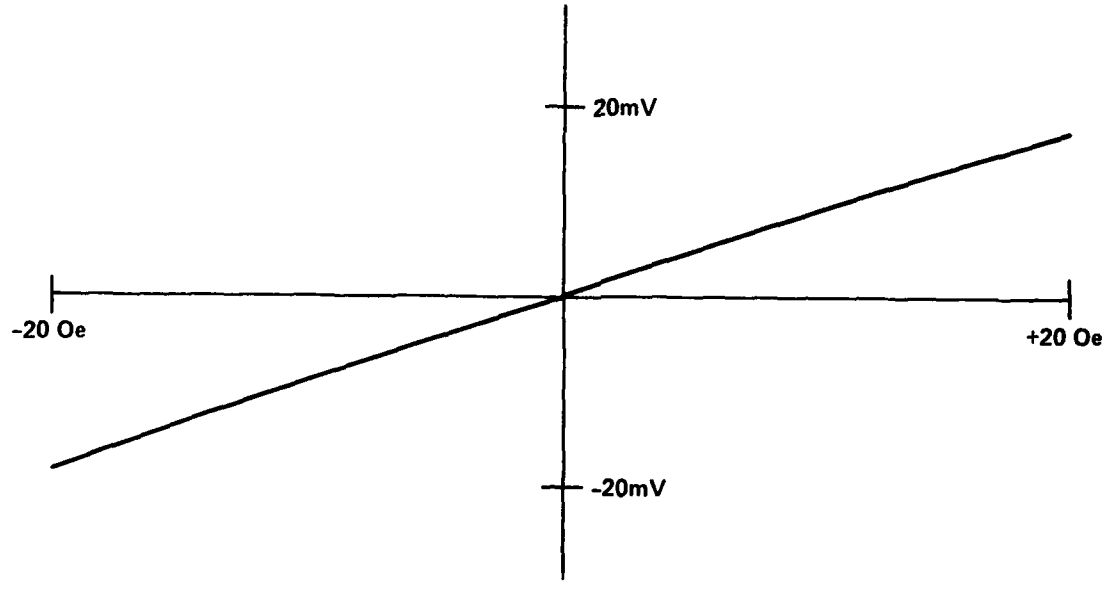

FIGURE 5-2. DYNAMIC RANGE OF THIN FILM MAGNETOMETER

CHAPTER 6

IMPROVEMENTS AND SUMMARY

In this final chapter, we wish to describe several areas which offer performance improvement. These areas can be classified as improvements in sensitivity, operational stability, power consumption and physical size.

PULSED MODE

In all the experiments described in Chapter Four, a constant DC current flowed through the bridge circuit, and the power consumption was a constant

$$\text{Power} = I_{\text{bridge}} \times V_{\text{bridge}}.$$

However, unless one has a need to instantaneously detect any change in a field level, one need not use the device in this DC mode. Rather, a pulsed mode is preferable. Using a clock and the appropriate gating logic, one could turn on the bridge for 1 millisecond and leave it in an off (zero bridge power consumption) state for 9 milliseconds, achieving a 10% duty cycle. Thus power consumption is reduced an order of magnitude with no loss in functionality. The power consumption of the drive circuitry can be made negligible if it is implemented in the appropriate technology.

MATERIALS

As we pointed out in Chapter Two, the sensitivity (and the figure of merit) of this magnetometer varies directly with the magnetoresistance ratio, $\Delta R/R_o$. Materials such as NiFeCo have been shown to have higher ratios than $Ni_{80}Fe_{20}$ and should be investigated further for magnetometers.

FULL BRIDGE CHIP

Incorporating all the legs of the bridge on a single chip is an obvious way to compact the detector. Figure 4-9 is a picture of an attempt to produce a bridge on a single substrate, but this was an adhoc effort. A genuine full bridge chip would need only four connections and have a square geometry. Of course, one must consider design constraints such as those discussed in Chapter Three.

BIAS FIELDS

The biasing techniques discussed so far in this report were limited to either large external coils or permanent magnets. Two other approaches can be envisioned, however. First, a layer of biasing material can be deposited during the fabrication process, thus integrating the source of the bias field with the three levels of the chip. This complicates the fabrication but simplifies assembly and increases the reliability. However, this must be pursued carefully so that the new deposition step does not degrade the results of the previous fabrication steps.

A second way of biasing involves wrapping the chip or chip carrier with strands of wire to enclose the chip in a coil This considerably complicates the assembly process, but offers a device with tunable sensitivity, as predicted by Figures 4-3 and 4-4. We note that it is a standard process to wrap bubble memory chips in two directions to supply the required rotating field necessary for operation, so packaging a magnetometer chip in a coil is certainly feasible.

HEAT SINKING

It is well known that the thermal conductivity of a silicon wafer exceeds that of glass by orders of magnitude. Thus depositing the sensor on silicon is an immediate improvement that can be made in reducing any self-heating that the sensor produces. This self-heating, produced by the current in the bridge, can be one source of thermal signal degradation, as discussed in Chapters Two and Four.

FLUX CONCENTRATORS

Other magnetometer designs have utilized flux concentrators which increase the flux density in the vicinity of the detector. This technique has improved the level of the minimal detectable field by several orders of magnitude.[7] Such a technique may be appropriate to our thin film magnetometer and should be pursued.

SUMMARY

In this report, we've presented the status of a project oriented towards producing a vector thin film magnetometer for use in military systems. In many respects, the theory and characterization of this device are well in hand. Possible improvements have been identified, but as the device exists today, it is suitable for applications such as discussed in Chapter Five. The improvements identified offer a device with features which will extend the range of possible applications.

REFERENCES

1. Cohen, M. S., "Ferromagnetic Properties of Films," in Handbook of Thin Film Technology, Maissel, L. I. and Glang, R., Ed., (New York: McGraw Hill Book Company, 1970), p. 17-27.

2. Cohen, p. 17-3.

3. Cohen, p. 17-7.

4. McQuire, T. R., and Potter, R. I., "Anisotropic Magnetoresistance in Ferromagnetic 3d Alloys," IEEE Trans. Magnetics, Vol. MAG-11, No. 4, Jul 1975, p. 1018.

5. Chi, G. C., et al., "The Magnetoresistiveity, Structure, and Magnetic Anisotropy of RF Sputtered and E-Beam Evaporated NiFe Films," J. Applied Physics, Vol. 52, No. 3, p. 2439.

6. Scarzello, J. F., et al., A Magnetic Coding Technique for Ordnance Round Identification (U), NSWC TR 80-459, May 1980 (Confidential).

7. Wieder, H. H., Hall Generators and Magnetoresistors, (London: "Pion Limited, 1971), p. 50.

DISTRIBUTION

	Copies
Defense Technical Information Center Cameron Station Alexandria, VA 22314	12
Commander Naval Sea Systems Command Attn: SEA-063R (F. J. Romano) PMS-407 (B. Kirk) SEA-62R1 (T. Tasaka) SEA-62R1 (C. Jedrey) SEA-63R1 (E. Liska) SEA-63R1 (D. Houser) SEA-06R (C.D. Smith) Washington, DC 20362	 2 1 1 1 1 1
Chief of Naval Operations Attn: NOP 374 NOP 009EB (R.K. Brooke) Washington, DC 20350	 1 1
Commander Mine Warfare Command Attn: Code 007 (S. Humphrey) Charleston, SC 29408	 2
Commander David W. Taylor Naval Ship R & D Center Attn: Code 2734 (W. J. Andahazy) Code 2734 (Bruce R. Hood) Code 2734 (E. Dadin) Annapolis, MD 21402	 1 1 1
Office of Naval Research Attn: Code 425GG (Dr. J. Heacock) Code 463 (R. Obrachta) 800 N. Quincy Street Arlington, Va 22217	 1 1
Library of Congress Attn: Gift and Exchange Division Washington, DC 20540	 4
Commander Naval Intelligence Support Center Attn: NISC 20 (G. Batts) 4301 Suitland Rd. Washington, DC 20390	 1
Commander Naval Air Development Center Attn: Code 3012 (E. Greeley) Code 3012 (P. Riemel) Code 5021 (R. Fedorak) Code 5021 (R. Josephs) Warminster, PA 18974	 1 1 1 1
Naval Research Laboratory Attn: Dr. J. Davis Dr. J. E. Wieselthier Washington, DC 20375	 1 1
U. S. Army Mobility Equipment R & D Center Attn: D. Keehan P. Hartman Ft. Belvoir, VA 22060	 1 1
U. S. Department of the Army Harry Diamond Laboratory Attn: B. Danner J. I. Cooperman Adelphi, MD 20783	 1 1
Institute of Geophysics and Planetary Physics University of California Space Sciences Center Attn: R. Snare Los Angeles, CA 90029	 1

DISTRIBUTION (Cont.)

	Copies
Goddard Space Flight Center Attn: Dr. M. Acuna Greenbelt, MD 20770	1
Federal Highway Administration Systems Technology Division Attn: M. K. Mills 6300 Georgetown Pike McLean, VA 22101	1
Infinetics, Inc. Attn: J. Jaquet P. O. Box 2330 201 Vander Avenue Wilmington, DE 19899	1
Spartan Electronics Corporation Attn: L. R. Staszak 2400 East Ganson Street Jackson, MI 49202	1
LaBarge, Inc. Electronics Division Attn: Richard Potts P. O. Box 926 Tulsa, OK 74101	1
Radio Corporation of America Attn: E. A. LeBlanc P. O. Box 588 Burlington, MA 01803	1
Army Research and Development Command Attn: Code DRDAR-LCU-PE (A. Schwartzman, Bldg. 1530) Dover, New Jersey 07801	1
Commander Naval Air Systems Command Attn: AIR 370 (B. Dillion) Washington, DC 20362	1

Internal Distribution	Copies
R	1
R40	1
R43	1
R43 (J. Scarzello)	1
R43 (A. Krall)	1
R45 (P. Hunter)	30
R45	1
R45 (L. Schwee)	20
R45 (F. Salton)	2
R45 (M. Shephard)	2
R45 (D. Gordon)	1
R45 (J. Cavallo)	1
R01	1
R04	1
U106	1
E06	1
E431	9
E432	3
G43 (C. Johnson)	1
TJ (J. Wynn)	1
R43 (D. Lenko)	1
R43 (J.R. Cunningham)	1
R43 (J. Skolnik)	1
U12 (V. Newton)	1
U12 (J. Sherman)	1
G43 (G. Briggs)	1
U12 (M. Meister)	1
U106 (B. DeSavage)	1
R43 (R. E. Brown)	1
E35 (GIDEP Office)	1